Competing orders in one-dimensional half-filled multicomponent fermionic cold atoms: The Haldane-charge conjecture

H. Nonne,[1] P. Lecheminant,[1] S. Capponi,[2] G. Roux,[3] and E. Boulat[4]

[1]*Laboratoire de Physique Théorique et Modélisation, CNRS UMR 8089, Université de Cergy-Pontoise, Site de Saint-Martin, F-95300 Cergy-Pontoise Cedex, France*

[2]*Laboratoire de Physique Théorique, CNRS UMR 5152, Université Paul Sabatier, F-31062 Toulouse, France*

[3]*Laboratoire de Physique Théorique et Modèles Statistiques, Université Paris-Sud, CNRS UMR 8626, F-91405 Orsay, France*

[4]*Laboratoire Matériaux et Phénomènes Quantiques, CNRS UMR 7162, Université Paris Diderot, F-75013 Paris, France*

(Received 18 July 2011; published 12 September 2011)

We investigate the nature of the Mott-insulating phases of half-filled $2N$-component fermionic cold atoms loaded into a one-dimensional optical lattice. By means of conformal field theory techniques and large-scale DMRG calculations, we show that the phase diagram strongly depends on the parity of N. First, we single out charged, spin-singlet degrees of freedom that carry a pseudospin $\mathcal{S} = N/2$, making it possible to formulate a Haldane conjecture: For attractive interactions, we establish the emergence of Haldane insulating phases when N is even, whereas a metallic behavior is found when N is odd. We point out that the $N = 1,2$ cases do *not* have the generic properties of each family. The metallic phase for N odd and larger than 1 has a quasi-long-range singlet pairing ordering with an interesting edge-state structure. Moreover, the properties of the Haldane insulating phases with even N further depend on the parity of $N/2$. In this respect, within the low-energy approach, we argue that the Haldane phases with $N/2$ even are not topologically protected but equivalent to a topologically trivial insulating phase and thus confirm the recent conjecture put forward by Pollmann *et al.* [arXiv:0909.4059 (to be published)].

DOI: 10.1103/PhysRevB.84.125123 PACS number(s): 71.10.Pm, 71.10.Fd, 03.75.Mn

I. INTRODUCTION

Topological phases have attracted much interest in recent years due to their robustness against perturbations and their relevance to quantum computation. A topological ordered phase is a gapped phase which displays a protected ground-state degeneracy dependent on the topology of the manifold in which the model is embedded.[1] This phase is not characterized by a local order parameter and falls beyond the usual symmetry-breaking paradigm of condensed-matter physics.[2]

One of the simplest examples of topologically ordered phases is the Haldane phase in quantum spin chains. In 1983, Haldane argued that the spin-S Heisenberg chain displays striking different properties depending on the parity of $2S$.[3] While half-integer Heisenberg spin chains have a gapless behavior, a finite gap from the singlet ground state (GS) to the first triplet excited states is found when $2S$ is even. On top of the existence of a gap, the spin-1 phase (the so-called Haldane phase) has remarkable exotic properties which may be regarded as manifestations of the existence of a topological ordered phase. This phase is not characterized by a local order but displays nonlocal string long-range ordering which signals the presence of a hidden Néel antiferromagnetic order.[4] The latter can be revealed through a nonlocal unitary transformation and the emergence of a complete breaking of a $\mathbb{Z}_2 \times \mathbb{Z}_2$ symmetry.[5] One remarkable resulting consequence of the Haldane phase is the liberation of fractional spin-1/2 degrees of freedom at the edge of the sample when the chain is doped by nonmagnetic impurities.[6]

Haldane's conjecture is now well understood and has been confirmed experimentally in quasi-one-dimensional (quasi-1D) compounds as well as numerically (see, for instance, Refs. 7 and 8). The Haldane phase displays unusual and interesting physical properties so that it is important to experimentally stabilize it in other contexts. In this respect, it has been argued that the Haldane phase is relevant to Josephson junction array systems.[9] Furthermore, it is likely that the Haldane physics will be explored experimentally in the near future in trapped ultracold atomic systems thanks to the tunability of interactions in these systems using optical lattices and Feshbach resonances. A first possible direction is to consider spin-1 bosons loaded into a 1D optical lattice with one atom per site so that the Haldane phase is one of the possible insulating phases of this model.[10] A second route consists in preparing 1D ultracold quantum gases with dipolar interactions, like ^{52}Cr bosonic atoms, where a Haldane insulating (HI) phase has been predicted.[11–14] Finally, we have recently shown that a similar phase can also be stabilized by considering 1D spin-3/2 cold fermions at half filling with *contact interactions only*.[15]

In this paper, we pursue our investigation of the HI phase in the context of 1D ultracold fermionic alkaline atoms in the general half-integer (hyperfine) spin $F = N - 1/2$ case at half filling (N atoms per site). In this respect, we use complementary analytical [renormalization group (RG) analysis, conformal field theory (CFT)[16]] and density-matrix renormalization group (DMRG)[17] techniques to fully determine the nature of the Mott-insulating phases at half filling when $N \geqslant 2$. The starting point of the analysis is the lattice model of $2N$ components cold fermions with contact interactions. Due to Pauli principle, low-energy s-wave scattering processes of spin-F fermionic atoms are allowed only in the even total spin $J = 0,2,\ldots,2N-2$ channels, so that the general effective Hamiltonian with

contact interactions reads as follows in absence of a magnetic field:[18]

$$\mathcal{H} = -t \sum_{i,\alpha} [c^\dagger_{\alpha,i} c_{\alpha,i+1} + \text{H.c.}] - \mu \sum_{i,\alpha} c^\dagger_{\alpha,i} c_{\alpha,i} + \sum_{i,J} U_J \sum_{M=-J}^{J} P^\dagger_{JM,i} P_{JM,i}, \quad (1)$$

where $c^\dagger_{\alpha,i}$ is the fermion creation operator corresponding to the $2N$ hyperfine states ($\alpha = 1, \ldots, 2N$) at the ith site of the optical lattice. The pairing operators in Eq. (1) are defined through the Clebsch-Gordan coefficients for spin-F fermions: $P^\dagger_{JM,i} = \sum_{\alpha\beta} \langle JM|F,F;\alpha\beta\rangle c^\dagger_{\alpha,i} c^\dagger_{\beta,i}$. In the general spin-$F$ case, there are N coupling constants U_J in model (1), which are related to the N two-body scattering lengths of the problem. In the following, in order to simplify the analysis of the Mott-insulating phases when $N > 2$, we perform a fine-tuning of the different scattering lengths in channels $J \geqslant 2$; that is, $U_2 = \ldots = U_{2N-2}$. Using the identity $\sum_{JM} P^\dagger_{JM,i} P_{JM,i} = n_i^2 - n_i$, model (1) can then be mapped onto the following:

$$\mathcal{H} = -t \sum_{i,\alpha} [c^\dagger_{\alpha,i} c_{\alpha,i+1} + \text{H.c.}] - \mu \sum_i n_i + \frac{U}{2} \sum_i n_i^2 + V \sum_i P^\dagger_{00,i} P_{00,i}, \quad (2)$$

with $U = 2U_2$ and $V = U_0 - U_2$, and $n_i = \sum_\alpha n_{\alpha,i} = \sum_\alpha c^\dagger_{\alpha,i} c_{\alpha,i}$ is the density at site i. In Eq. (2), the singlet BCS pairing operator for spin-F fermions is $\sqrt{2N} P^\dagger_{00,i} = \sum_{\alpha\beta} c^\dagger_{\alpha,i} \mathcal{J}_{\alpha\beta} c^\dagger_{\beta,i} = -\sum_\alpha (-1)^\alpha c^\dagger_{\alpha,i} c^\dagger_{2N+1-\alpha,i}$, the matrix $\mathcal{J}$ being a $2N \times 2N$ antisymmetric matrix with $\mathcal{J}^2 = -I$. When $N = 1$, $P^\dagger_{00,i}$ coincides with the Cooper pairing $c^\dagger_{\uparrow,i} c^\dagger_{\downarrow,i}$ so that model (2) is equivalent to the spin-1/2 Hubbard model.

Model (2) obviously conserves the total number of fermions – no atoms are dynamically created or annihilated. This conservation law is associated to a U(1) continuous symmetry $c_{\alpha,i} \to e^{i\theta} c_{\alpha,i}$, which, by analogy with condensed matter dealing with electrons, we will refer to as a "U(1)$_c$ charge symmetry," the charge being simply the number of fermions. On top of this symmetry, model (2) displays an extended continuous symmetry for $N > 1$ in spin space. When $V = 0$ ($U_0 = U_2$) model (2) is the Hubbard model for $2N$-component fermions with a U($2N$) = U(1)$_c \times$ SU($2N$) invariance. The Hamiltonian (2) for $V \neq 0$ still displays an extended symmetry since the BCS singlet-pairing operator $P^\dagger_{00,i}$ is invariant under the Sp($2N$) group, which consists of $2N \times 2N$ unitary matrices U that satisfy $U^* \mathcal{J} U^\dagger = \mathcal{J}$. When $V \neq 0$, the continuous symmetry of model (2) is thus U(1)$_c \times$ Sp($2N$).[19,20] In the $F = 3/2$ case, that is, $N = 2$, there is no fine-tuning; models (1) and (2) are equivalent and share an exact Sp(4) $\simeq$ SO(5) spin symmetry.[21] The zero-temperature phase diagram of model (2) away from half filling has been investigated by means of a low-energy approach[22–24] in the general N case and by quantum Monte Carlo and DMRG calculations for $N = 2$.[25,26] A rich exotic physics emerge when $N \geqslant 2$ with, in particular, the stabilization of a superconducting instability with charge $2Ne$ for attractive interactions and at sufficiently low density.[22–25]

At half filling (when $\mu = NU + V/N$), model (2) enjoys a particle-hole symmetry $c_{\alpha,i} \to (-1)^i \sum_\beta \mathcal{J}_{\alpha\beta} c^\dagger_{\beta,i}$, which plays a crucial role in the following. In the $N = 1$ case, it is well known that the particle-hole symmetry enlarges the U(1)$_c$ charge symmetry of the spin-1/2 Hubbard model to an SU(2)$_c$ symmetry at half filling.[27,28] In addition, the physics of the half-filled spin-1/2 Hubbard model for repulsive and attractive interactions are related through a canonical transformation $c_{\uparrow,i} \to (-1)^i c^\dagger_{\uparrow,i}$, $c_{\downarrow,i} \to c_{\downarrow,i}$. While for $U > 0$ a Mott-insulating phase with one gapless spin mode is stabilized, there is a spin gap for attractive interaction which marks the emergence of a singlet-pairing phase.[29,30] When $N > 1$, all these properties do not generalize; in particular, the symmetry enlargement of the charge degrees of freedom at half filling requires an additional fine tuning $V = NU$ to display an SU(2)$_c \times$ Sp($2N$) global invariance.[15] We have shown in Ref. 15 that this SU(2)$_c$ symmetry is central to the emergence of an even-odd scenario for attractive interactions in close parallel to the famous Haldane conjecture in spin-S SU(2) Heisenberg chains. In this respect, we have identified a spin-singlet pseudospin $N/2$ operator which governs the low-energy properties of the model in the vicinity of the SU(2)$_c$ line for attractive interactions. This operator gives rise to a Haldane-charge conjecture with the emergence of a HI phase when N is even, while a metallic phase is stabilized when N is odd. Such a scenario has been checked in Ref. 15 by a low-energy approach in the $N = 2$ case and DMRG calculations for $N = 2,3$ in the vicinity of the SU(2)$_c$ line. In the special $N = 2$ case, these complementary techniques reveal unambiguously the existence of a HI phase with nonlocal string charge correlations and pseudo-spin-1/2 edge states.

In this paper, we extend the results of our letter Ref. 15 by determining the zero-temperature phase diagram of model (2) at half filling by means of a low-energy approach in the general N case and DMRG calculations for $N = 2,3,4$. On top of the confirmation of the Haldane-charge conjecture, we show that the $N = 1$ and $N = 2$ cases are special and are not the generic cases of each family. In particular, for $N > 1$ odd, the metallic phase with dominant singlet-pairing correlation has an interesting edge-state structure when open-boundary conditions (OBC) are used, similarly to the spin-3/2 Heisenberg chain.[31,32] For all N even > 2, a new gapless phase with dominant singlet-pairing instability is stabilized between the HI phase and the rung-singlet (RS) phase. In addition, we show, within the low-energy approach, that the HI phase has striking different properties depending on the parity of $N/2$. When $N/2$ is even, the HI phase turns out to be equivalent to the topologically trivial RS insulating phase whereas it is a topologically ordered phase when $N/2$ is odd in full agreement with the recent findings in the study of integer Heisenberg spin chains.[33,34]

The rest of the paper is organized as follows. In Sec. II, we discuss the strong-coupling analysis of model (2) along special highly symmetric lines which give some clues about the nature of the Mott-insulating phases. The low-energy approach of the general N case is presented in Sec. III. In Sec. IV, we map

out the phase diagram of model (2) with $N = 2$ by means of intensive DMRG calculations. Sections V and VI describe our DMRG results, respectively, for the $N = 3,4$ cases to complement the low-energy approach. Finally, our concluding remarks are given in Sec. VII.

II. STRONG-COUPLING ANALYSIS

Before investigating the zero-temperature phase diagram of model (2) by means of the low-energy and DMRG approaches, a strong-coupling analysis along the highly symmetric lines of the model might be useful to shed light on the possible Mott-insulating phases. To this end, let us first consider the energy spectrum for the single-site problem.

The Hubbard term of Eq. (2) distributes the different states into energy levels with the same number of particles n, with $n = 0,\ldots,2N$; this is the one-site spectrum of the U($2N$) Hubbard model. The singlet-pairing term in Eq. (2) with coupling constant V will split these levels into levels with different pairing schemes, denoted (n,k). The level (n,k) group states with n particles, among which $2k$ particles are in k Sp($2N$) singlets. These states transform in the $\bar{\omega}_{n-2k}$ representation of Sp($2N$). Note that, for a given number of particles n, $0 < k < E(n/2)$ if $n \leqslant N$, and $n - N < k < E(n/2)$ if $n > N$, where $E(x)$ is the floor function. In order to write down the eigenstates in terms of fermionic operators, let us define the pair operator that creates a pair of fermions with spins α and $2N + 1 - \alpha$ by

$$P^{\dagger}_{\alpha,i} = c^{\dagger}_{\alpha,i} c^{\dagger}_{2N+1-\alpha,i}. \tag{3}$$

In terms of these operators, the singlet pairing operator $P^{\dagger}_{00,i}$ is

$$P^{\dagger}_{00,i} = \frac{-2}{\sqrt{2N}} \sum_{\alpha=1}^{N} (-1)^{\alpha} P^{\dagger}_{\alpha,i}. \tag{4}$$

We now need to define a set of $N - 1$ linear combinations of $P^{\dagger}_{\alpha,i}$ "orthogonal" to $P^{\dagger}_{00,i}$ that we label as $\Pi^{\dagger}_{l,i}$ (with $l = 1,\ldots,N-1$). The $n - 2k$ particles that are not Sp($2N$) singlets then divide into two kinds: They can be either written as linear combinations of pairs of particles with spin $(\alpha, 2N + 1 - \alpha)$ and thus as a combination of pair operators $\Pi^{\dagger}_{l,i}$, or they are unpaired and can be only written with a single creation operator $c^{\dagger}_{\alpha,i}$. In the end, the eigenstates that belong to the energy level (n,k) are written as

$$|n;k,m\rangle = \frac{1}{\mathcal{M}_{n,k,m}} c^{\dagger}_{\alpha_1,i} \ldots c^{\dagger}_{\alpha_p,i} \Pi^{\dagger}_{l_1} \ldots \Pi^{\dagger}_{l_q} (P^{\dagger}_{00,i})^k |0\rangle, \tag{5}$$

where m labels the state, $\mathcal{M}_{n,k,m}$ is a normalization factor, p is the number of "single" particles, and $2q$ is the number of "paired" particle that cannot be penned down in terms of $P^{\dagger}_{00,i}$. The energy of the eigenstates (5) only depends on (n,k) and reads

$$E(n,k) = \frac{n^2}{2} U + \left[2k \left(1 + \frac{k+1}{N} - \frac{n}{N} \right) \right] V - n\mu. \tag{6}$$

The energy level (n,k) is $\mathcal{D}(n,k)$-fold degenerate, with

$$\mathcal{D}(n,k) = \frac{2(N - n + 2k + 1)(2N + 1)!}{(n - 2k)!(2N - n + 2k + 2)!}. \tag{7}$$

At half filling, μ is set by the particle-hole symmetry: $\mu = NU + V/N$, and the energy levels read

$$E(n,k) = \left(\frac{n^2}{2} - nN \right) U + \left[2k \left(1 + \frac{k+1}{N} - \frac{n}{N} \right) - \frac{n}{N} \right] V. \tag{8}$$

At this point, we can consider two important highly symmetric lines for all N: $V = 0$ (respectively, $V = NU$) with the emergence of a U($2N$) [respectively, SU(2)$_c$ × Sp($2N$)] extended symmetry. We also mention that in the special $N = 2$ case, there is an additional SO(7) symmetric line at half filling when $V = -2U$.[21] However, despite the fact that we indeed find an additional degeneracy for the one-site problem in the general N case on the special line $V = -N^2U/2$, the latter seems not to correspond to an enlarged symmetry since the kinetic term lifts it.

A. Strong-coupling argument close to the $V = 0$ line

When $V = 0$, as already stated in the Introduction, model (2) is equivalent to the U($2N$) Hubbard model. The degeneracies of the energy-spectrum (8) with $V = 0$ are related to the dimensions of representations of the SU($2N$) group. In particular, when $U > 0$, we observe from Eq. (8) that the lowest-energy states correspond to $n = N$ and transform in the antisymmetric self-conjugate representations of SU($2N$) (representation described by a Young tableau with one column of N boxes). This case has been studied in Ref. 35 and in the strong coupling limit the model is equivalent to an SU($2N$) Heisenberg spin chain where the spin operators belong to the antisymmetric self-conjugate representation of SU($2N$). The latter model is expected to have a dimerized or Spin-Peierls (SP) twofold degenerate GS, where dimers are formed between two neighboring sites.[35,36] In the $N = 2$ [i.e., SU(4)], such a SP phase has been ascertained by means of a low-energy approach, quantum Monte Carlo, and DMRG calculations.[37–40] The strong U limit gives the opportunity to get a simple physical picture of the GS, as well as of the low-lying excitations. The twofold degenerate GS allows for *kink* configurations that interpolate between the two vacua. As depicted in Fig. 1, these kinks have zero charge but carry a nonzero SU($2N$) spin since they transform in the antisymmetric self-conjugate representation of SU($2N$). Note that the system also allows for *charged* kinks, that carry charge $Q_k = k - N$ with $k = 0,\ldots,2N$. These states transform in ω_k, the antisymmetric representation of SU($2N$) with Young tableau made of a single column with k boxes. Although at large U they are expected to have a large gap of order $\Delta_k \sim U\,(N-k)^2/2$ as seen from (8), we nevertheless introduce them here since they will play an important role at small U (see Sec. III C). Notice also that these kink excitations have a collective nature; that is, their quantum number cannot be reproduced by states built by using a finite number of fermions.

In the attractive case ($U < 0$), the lowest energy states are the empty and the fully occupied state, which is an SU($2N$)

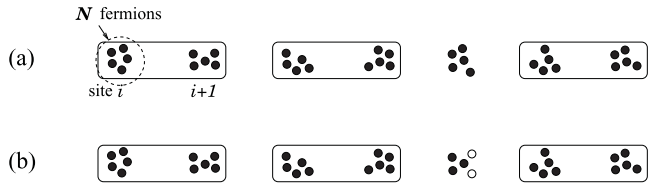

FIG. 1. Sketch of the kinks supported by the U($2N$) repulsive Hubbard model that interpolate between the two degenerate dimerized vacua [the boxes indicate an SU($2N$) singlet made of $2N$ fermions]. Here $N = 5$. At large U, in the low-energy sector, all sites have exactly N fermions. (a) Neutral kinks, that are the only low-energy excitations at large U, and transform in the antisymmetric representation ω_N. Note that they are their own antiparticle. (b) Charged kinks, that play a role at small U, depicted here with charge $Q = -2$.

[and Sp($2N$) as well] singlet. At second order of perturbation theory, the effective model is thus[41]

$$\mathcal{H}_{\text{eff}} = \frac{t^2}{N(2N-1)|U|}\sum_i (n_i n_{i+1} - N n_i). \tag{9}$$

The first term introduces an effective repulsion interaction between nearest-neighbor sites. This leads to a fully gapped charge-density wave (CDW) where empty and fully occupied states alternate. This phase has a long-range order and is twofold degenerate.

B. Strong-coupling argument close to the $V = NU$ line

The second highly symmetric line corresponds to the additional SU$(2)_c$ symmetry in the charge sector for $V = NU$ that we have identified in Ref. 15. On this line, one easily verifies from Eq. (8) that all pure $(P^\dagger_{00,i})^k$ states (i.e., the states with $n = 2k, k = 0, \ldots, N$) are degenerate, with energy $E = 0$. Let us give the proper normalization factor for these states:

$$\begin{aligned} \left|P^k_{00,i}\right\rangle &= \frac{1}{\mathcal{M}(k)}(P^\dagger_{00,i})^k|0\rangle, \\ \text{with}\quad \mathcal{M}(k) &= \sqrt{\left(\frac{2}{N}\right)^k\left(\prod_{q=0}^{k-1}(k-q)(N-q)\right)}. \end{aligned} \tag{10}$$

They transform in the spin-$N/2$ representation of SU(2) and we define the corresponding pseudospin operator acting on them as

$$\begin{aligned} \mathcal{S}^\dagger_i &= \sqrt{N/2}P^\dagger_{00,i}, \\ \mathcal{S}^z_i &= (n_i - N)/2. \end{aligned} \tag{11}$$

This operator carries charge and is a Sp($2N$) spin-singlet. It generalizes the η-pairing operator introduced by Yang for the half-filled spin-1/2 (i.e., $N = 1$) Hubbard model[27] or by Anderson in his study of the BCS superconductivity.[42] It is easy to observe that $\vec{\mathcal{S}}_i$ satisfies the SU(2) commutation relations; $\mathcal{S}^\dagger_i$ allows to construct the whole set of states with $E = 0$ from $|0\rangle$ with

$$\begin{aligned} \mathcal{S}^\dagger_i\left|P^k_{00,i}\right\rangle &= \sqrt{(N-k)(k+1)}\left|P^{k+1}_{00,i}\right\rangle, \\ \mathcal{S}^-_i\left|P^k_{00,i}\right\rangle &= \sqrt{k(N-k+1)}\left|P^{k-1}_{00,i}\right\rangle. \end{aligned} \tag{12}$$

Let us check the commutation relation of $\vec{\mathcal{S}}$ with the Hamiltonian. For the interacting part alone ($\mathcal{H}_{\text{int}} = \mathcal{H}[t = 0]$), we have (for a generic filling)

$$\begin{aligned} [\mathcal{H}_{\text{int}}, \mathcal{S}^\dagger_i] &= \left[-2\mu - 2U + \frac{2V}{N}(N+2) \right. \\ &\quad \left. + 2\left(U - \frac{V}{N}\right)n_i\right]\mathcal{S}^\dagger_i, \\ [\mathcal{H}_{\text{int}}, \mathcal{S}^z_i] &= 0, \end{aligned} \tag{13}$$

so that they commute only at half filling and when $V = NU$; as for the hopping term, $\mathcal{H}_t = -t\sum_{i,\alpha}(c^\dagger_{\alpha,i}c_{\alpha,i+1} + \text{H.c.})$, it commutes with the total charge pseudospin operator if we define it as

$$\begin{aligned} \mathcal{S}^\dagger &= \sum_i (-1)^i \mathcal{S}^\dagger_i, \\ \mathcal{S}^z &= \sum_i \mathcal{S}^z_i. \end{aligned} \tag{14}$$

The pseudospin operator thus generates a higher SU$(2)_c \times$ Sp($2N$) symmetry at half filling along the line $V = NU$ and we can recast the interacting (on-site) Hamiltonian as $\mathcal{H}_{\text{int}} = 2U\sum_i[\vec{\mathcal{S}}^2_i - N(N+2)/4]$; the pseudospin $\vec{\mathcal{S}}_i$ is a spin-$N/2$ operator. The existence of such an extended SU(2) symmetry in the charge sector for $N = 2$ has been first noticed in Ref. 43.

For a strong attractive U, one can derive an effective Hamiltonian in the strong-coupling regime $|U| \gg t$ using the standard strategy.[44] To second order of perturbation theory, one obtains the effective model:

$$\mathcal{H}_{\text{eff}} = \sum_i \left(J\vec{\mathcal{S}}_i \cdot \vec{\mathcal{S}}_{i+1} + D\left(\mathcal{S}^z_i\right)^2\right), \tag{15}$$

with

$$\begin{aligned} J &= \frac{4t^2}{N(2N+1)|U|}, \\ D &= 2\left(U - \frac{V}{N}\right). \end{aligned} \tag{16}$$

On the SU$(2)_c$ symmetric line ($V = NU$), $D = 0$, and model (15) is the spin-$N/2$ antiferromagnetic SU(2) Heisenberg chain. From this strong-coupling approach, we thus expect the emergence of an even-odd dichotomy for attractive interactions along the SU(2) line. For even N, that is, integer pseudospin, the HI phase is formed while a metallic phase is stabilized when N is odd, that is, half-integer pseudospin. This is the same as Haldane's conjecture for model (15) except that the underlying spin $\vec{\mathcal{S}}$ is nonmagnetic and carries charge. In this respect, we coin it Haldane-charge conjecture. When we deviate from this SU$(2)_c$ line, the SU$(2)_c$ charge symmetry is broken down to U$(1)_c$ and the single-ion anisotropy appears. The phase diagram of the resulting model for general N is known from the bosonization work of Schulz.[45] For even

N, on top of the Haldane phase, Néel and large-D singlet gapful phases appear. Using the expression of the pseudospin operator (11), the Néel and large-D singlet phases correspond, respectively, to the CDW and RS phases. When N is odd, gapless (XY) and gapful (Ising) phases are stabilized in the vicinity of the SU(2) line. The gapless XY phase can be viewed as singlet-pairing phase since $\mathcal{S}_i^\dagger \sim P_{00,i}^\dagger$.

III. LOW-ENERGY APPROACH

In this section, we present the low-energy description of the model (2) in the general N case. This will lead us to map out the phase diagram at zero temperature and to show the emergence of the Haldane-charge conjecture in the weak-coupling limit. As will be shown, the $N = 2$ case, which was already presented in Ref. 15, turns out to be very particular and is not the generic case of the even N family.

A. Continuum limit

The low-energy effective field theory of the lattice model (2) is derived by taking the standard continuum limit of the lattice fermionic operators $c_{\alpha i}$, written in terms of left- and right-moving L_α, R_α Dirac fermions:[29,30]

$$\frac{c_{\alpha i}}{\sqrt{a_0}} \to R_\alpha e^{ik_F x} + L_\alpha e^{-ik_F x}, \tag{17}$$

with $x = ia_0$ (a_0 being the lattice spacing) and $k_F = \pi/(2a_0)$ is the Fermi momentum. In the continuum limit, the noninteracting part of the Hamiltonian (2) corresponds to the Hamiltonian density of $2N$ free relativistic massless fermions:

$$\mathcal{H}_0 = -iv_F(R_\alpha^\dagger \partial_x R_\alpha - L_\alpha^\dagger \partial_x L_\alpha), \tag{18}$$

where $v_F = 2ta_0$ is the Fermi velocity and we assume in the following a summation over repeated indices. The continuous symmetry of the noninteracting part of the model is enlarged to $\mathrm{SO}(4N)|_L \times \mathrm{SO}(4N)|_R$ since $2N$ complex (Dirac) fermions are equivalent to $4N$ real (Majorana) fermions. This SO($4N$) symmetry is the maximal continuous symmetry of $2N$ Dirac fermions. The corresponding CFT is the $\mathrm{SO}(4N)_1$ with central charge $c = 2N$.[16]

The crucial point is now to find a good basis describing the low-energy properties of the model. Some simple considerations on its symmetries guide us to choose the relevant conformal embedding of the problem. No spin-charge separation at half filling is expected for $N > 1$, and since the global symmetry invariance of model (2) is Sp($2N$), we need to understand how the noninteracting conformal symmetry $\mathrm{SO}(4N)_1$ decomposes into $\mathrm{Sp}(2N)_1$ CFT. The general list of conformal embeddings can be found in Ref. 46 and the one which is directly relevant to our problem is:[47]

$$\mathrm{SO}(4N)_1 \sim \mathrm{SU}(2)_N \times \mathrm{Sp}(2N)_1, \tag{19}$$

where the $\mathrm{SU}(2)_N$ [respectively, $\mathrm{Sp}(2N)_1$] CFT has central charge $c = 3N/(N+2)$ [respectively, $c = N(2N+1)/(N+2)$].

The next step of the approach is to express the $2N(4N-1)$ $\mathrm{SO}(4N)_1$ currents, which are made from all Dirac fermionic bilinears, in terms of the currents of the $\mathrm{SU}(2)_N$ and $\mathrm{Sp}(2N)_1$ CFTs, in order to write down the effective interacting Hamiltonian in the new basis. To this end, let us consider the following left currents which appear in the low-energy description of the model away from half filling:[22,23]

$$\begin{aligned} J_L^A &= L_\alpha^\dagger T_{\alpha\beta}^A L_\beta, \text{ the } \mathrm{SU}(2N)_1 \text{ spin currents,} \\ J_L^a &= L_\alpha^\dagger T_{\alpha\beta}^a L_\beta, \text{ the } \mathrm{Sp}(2N)_1 \text{ spin currents,} \\ J_L^i &= L_\alpha^\dagger T_{\alpha\beta}^i L_\beta, \text{ the } \mathrm{SU}(2N)_1/\mathrm{Sp}(2N)_1 \text{ currents,} \end{aligned} \tag{20}$$

where T^A are the $4N^2-1$ SU($2N$) generators in the fundamental representation, T^a being the $N(2N+1)$ Sp($2N$) generators in the fundamental representation, and T^i are the $2N^2-N-1$ remaining generators of SU($2N$). All these generators are normalized in such a way that they satisfy $\mathrm{Tr}(T^A T^B) = \delta^{AB}/2$. We need then to introduce the $\mathrm{SU}(2)_N$ currents to complete the conformal embedding. In this respect, one may use the recognition of the SU(2) pseudospin operator (11) to consider the following left current:

$$\begin{aligned} \mathcal{J}_L^\dagger &= \tfrac{1}{2}\, L_\alpha^\dagger J_{\alpha\beta} L_\beta^\dagger, \\ \mathcal{J}_L^z &= \tfrac{1}{2}\, :L_\alpha^\dagger L_\alpha:, \end{aligned} \tag{21}$$

where :: stands for the normal ordering with respect to the Fermi sea of the noninteracting theory. Note the unusual definition of the charge current $\mathcal{J}_L^z$; the 1/2 factor in Eq. (21) is there to realize the $\mathrm{SU}(2)_N$ algebra:[48]

$$\mathcal{J}_L^a(z)\mathcal{J}_L^b(0) \sim \frac{N\delta^{ab}}{8\pi^2 z^2} + \frac{i\epsilon^{abc}}{2\pi z}\mathcal{J}_L^c(0), \tag{22}$$

with $a,b = 1,2,3$ and $z = v_F\tau + ix$ (τ being the imaginary time).

At this point, we have only defined $4N^2+2$ currents, and we now have to introduce the $4N^2-2N-2$ other pseudocurrents in order to take into account the umklapp terms of the form $K_\alpha^\dagger K_\beta^\dagger, K_\alpha K_\beta$ ($K = L, R$). In this respect, let us consider

$$J_L^{i+} = L_\alpha^\dagger \tilde{T}_{\alpha\beta}^i L_\beta^\dagger, \tag{23}$$

where the generators $\tilde{T}_{\alpha\beta}^i$ are such that, together with $J_{\alpha\beta}$, they form the set of antisymmetric generators of SU($2N$); there are $N(2N-1)-1$ of them, so that all the left $2N(4N-1)$ $\mathrm{SO}(4N)_1$ currents are described by $J_L^a, J_L^i, \mathcal{J}_L^\pm, \mathcal{J}_L^z, J_L^{i\pm}$, with $a = 1,\ldots,N(2N+1)$ and $i = 1,\ldots,2N^2-N-1$.

With these currents at hand, we can now derive the low-energy effective expression of the interacting part of model (2) at half filling. The interacting part of this low-energy Hamiltonian can then be deduced by symmetry, simply by requiring the Sp($2N$) invariance:

$$\begin{aligned} \mathcal{H}_{\mathrm{int}} = {} & g_1 J_R^a J_L^a + g_2 J_R^i J_L^i + g_3 \mathcal{J}_R^z \mathcal{J}_L^z + \frac{g_4}{2}\left(J_R^{i+} J_L^{i-} + \mathrm{H.c.}\right) \\ & + \frac{g_5}{2}(\mathcal{J}_R^+ \mathcal{J}_L^- + \mathrm{H.c.}), \end{aligned} \tag{24}$$

where we have neglected four-fermion chiral interactions which would only introduce a velocity anisotropy. A direct

continuum limit leads to the identification:

$$g_1 = -a_0\left(2U + \frac{4V}{N}\right),$$
$$g_2 = -a_0\left(2U - \frac{4V}{N}\right),$$
$$g_3 = \frac{2}{N}a_0\left(U(2N-1) + \frac{2V}{N}\right), \quad (25)$$
$$g_4 = 2Ua_0,$$
$$g_5 = \frac{2}{N}a_0(U+2V).$$

Along the U($2N$) line with $V = 0$, we have $g_1 = g_2 = -\frac{N}{2N-1}g_3 = -g_4 = -Ng_5$. When $V = NU$, model (24) displays a manifest SU$(2)_c \times$ Sp($2N$) invariance with $g_2 = g_4$ and $g_3 = g_5$. The interaction of model (24) is marginal, so that a one-loop RG analysis can be performed to deduce its low-energy properties.

B. Phase diagram for $N = 2$

The RG analysis for $N = 2$ has been presented in details in Refs. 15 and 40. For completeness and especially for the comparison with the DMRG calculations of Sec. IV, we give here a brief account of the main results of this case.

Since Sp$(4)_1 \sim$ SO$(5)_1$ and SU$(2)_2 \sim$ SO$(3)_1$, the currents in Eq. (24) admit a free-field representation in terms of eight Majorana fermions: $\xi^a_{R,L}, a = 1,\ldots,5$ describe the fluctuations of the Sp(4) spin degrees of freedom whereas $\xi^{6,7,8}_{R,L}$ account for the remaining ones. The interacting Hamiltonian (24) reads as follows in terms of these Majorana fermions:

$$\mathcal{H}_{\rm int} = \frac{g_1}{2}\left(\sum_{a=1}^{5}\xi^a_R\xi^a_L\right)^2 + g_2\,\xi^6_R\xi^6_L\sum_{a=1}^{5}\xi^a_R\xi^a_L + \frac{g_3}{2}\left(\xi^7_R\xi^7_L + \xi^8_R\xi^8_L\right)^2 + \left(\xi^7_R\xi^7_L + \xi^8_R\xi^8_L\right) \times \left(g_4\sum_{a=1}^{5}\xi^a_R\xi^a_L + g_5\,\xi^6_R\xi^6_L\right). \quad (26)$$

One particularity of the Majorana fermion basis is that it allows for a very simple representation of nonperturbative hidden duality symmetries in the low-energy effective Hamiltonian (26). These discrete symmetries are very useful to determine the zero-temperature phase diagram.[49] For model (26), we can define two independent duality symmetries:

$$\Omega_1 \;:\; \xi^{7,8}_L \to -\xi^{7,8}_L$$
$$\Omega_2 \;:\; \xi^6_L \to -\xi^6_L, \quad (27)$$

while the right-moving fermions remain invariant. The transformations (27) are exact symmetries of Eq. (26) if the couplings are simultaneously changed according to $g_{4,5} \to -g_{4,5}$ for Ω_1, and $g_{2,5} \to -g_{2,5}$ for the second duality Ω_2. These duality symmetries along with the one-loop RG equations enable us to map out the phase diagram of the $N = 2$ case. This analysis has been done in Refs. 15 and 40 and we find four insulating phases in the phase diagram, depicted in Fig. 2.

A first twofold degenerate phase, which contains the SU(4) line with repulsive U, is a SP phase with a nonzero order parameter $\mathcal{O}_{\rm SP} = \sum_\alpha (-1)^i c^\dagger_{\alpha,i+1}c_{\alpha,i}$. The duality symmetry

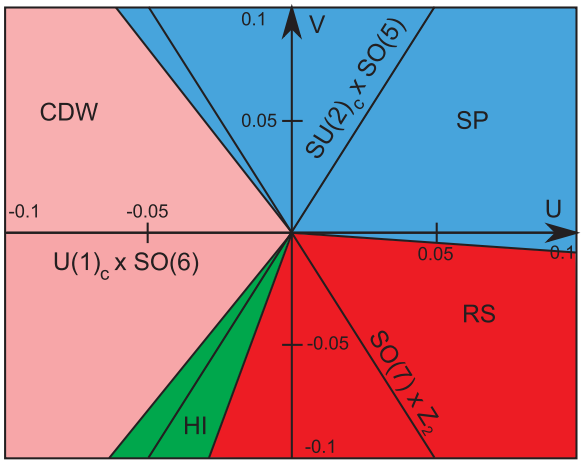

FIG. 2. (Color online) Phase diagram obtained by the low-energy approach in the $N = 2$ case.

Ω_1 gives a second gapful twofold degenerate phase which is a CDW phase with order parameter $\mathcal{O}_{\rm CDW} = \sum_\alpha (-1)^i c^\dagger_{\alpha,i}c_{\alpha,i}$. This phase contains the SU(4) line with negative U, in full agreement with the numerical result of Ref. 41. On top of these twofold degenerate phases, there are two nondegenerate insulating phases which are stabilized with help of the Ω_2 duality symmetry. Starting from the CDW phase and applying the Ω_2 transformation, one obtains a HI phase which includes the SU$(2)_c$ line $V = 2U$ with attractive U. This gapful nondegenerate phase is equivalent to the Haldane phase of the spin-1 Heisenberg chain and displays a hidden ordering which can be revealed through a nonlocal string order parameter. This order parameter is built from the pseudospin operator (11) and the HI phase is characterized by the long-range ordering:

$$\lim_{|i-j|\to\infty}\langle \mathcal{S}^z_i e^{i\pi\sum_{k=i+1}^{j-1}\mathcal{S}^z_k}\mathcal{S}^z_j\rangle \neq 0. \quad (28)$$

As a consequence of this ordering, this phase displays pseudospin-1/2 edge states which carry charge but are spin-singlet states (holon edge states).[15] Finally, the last insulating phase is obtained from this HI phase by applying the Ω_1 duality. One obtains a gapful nondegenerate RS phase, equivalent to the RS phase of the two-leg spin ladder with antiferromagnetic interchain coupling.[29,30] This RS phase has no edge states and is characterized by the string ordering:[15]

$$\lim_{|i-j|\to\infty}\langle e^{i\pi\sum_{k=i+1}^{j-1}\mathcal{S}^z_k}\rangle \neq 0. \quad (29)$$

Finally, the different quantum phase transitions of Fig. 2 can also be determined by means of the duality symmetries (27). The transitions SP/CDW and HI/RS are Berezenskii-Kosterlitz-Thouless (BKT) transitions with central charge $c = 1$, whereas SP/RS and CDW/HI transitions belong to the 2D Ising universality class with central charge $c = 1/2$.

C. Renormalization group analysis: General N case

We now turn to the general $N > 2$ case, which is much more involved. The leading effects of the current-current interaction of model (24) can be inferred from a one-loop RG approach. In this respect, it is useful to rescale the coupling constants

as $g_{1,2,4} \to 2\pi v_F N g_{1,2,4}$ and $g_{3,5} \to 2\pi v_F g_{3,5}$ to obtain the one-loop RG equations:

$$\begin{aligned} \dot{g_1} &= \frac{N}{2}\left[(N+1)g_1^2 + (N-1)g_2^2 + 2(N-1)g_4^2\right], \\ \dot{g_2} &= N^2 g_1 g_2 + (N^2 - N - 2)g_4^2 + 2g_4 g_5, \\ \dot{g_3} &= (2N^2 - N - 1)g_4^2 + g_5^2, \\ \dot{g_4} &= N^2 g_1 g_4 + (N^2 - N - 2)g_2 g_4 + g_3 g_4 + g_2 g_5, \\ \dot{g_5} &= (2N^2 - N - 1)g_2 g_4 + g_3 g_5, \end{aligned} \tag{30}$$

where $\dot{g}_i = \partial g_i / \partial l (i = 1, \ldots, 5)$, l being the RG time.

Here we remark the particular character of the case $N = 2$, where the term in $N^2 - N - 2$ cancels out in the equation for g_2 and g_4. It is this very term that makes the general N case tricky. Indeed, because of it, the duality symmetry Ω_2 of the $N = 2$ case (27) disappears for $N > 2$ and, with it, fades out in a very satisfactory way to precisely identify and characterize the different phases in the phase diagram. The only duality symmetry Ω_1 which remains when $N > 2$ corresponds to the transformation $L_\alpha \to i L_\alpha$ on the left-moving Dirac fermions, so that

$$\Omega_1 : \mathcal{J}_L^{\pm} \to -\mathcal{J}_L^{\pm}, \quad J_L^{i\pm} \to -J_L^{i\pm}, \tag{31}$$

while the other currents are invariant. Thus, the duality transformation Ω_1 is an exact symmetry of model (24) when $g_{4,5} \to -g_{4,5}$. In particular, the RG Eqs. (30) are indeed symmetric with respect to $g_{4,5} \to -g_{4,5}$.

We have solved numerically the RG equations by a standard Runge-Kutta method. In order to have a picture of the RG flow, it is useful to draw diagrams on a ring defined by $R^2 = U^2 + V^2, U = R\cos\theta, V = R\sin\theta$ with $\theta = 0 \ldots 2\pi$; in our numerical calculations, we set $R = 0.1t$. The procedure is the following: We initiate the couplings g_i for a given value of θ and run the Runge-Kutta algorithm on the RG Eqs. (30). The coupling constants g_i flow to the strong coupling regime under RG time so we need to stop the procedure at one point. To this end, we stop the RG iterations as soon as one of the couplings reaches a limit value G; this happens at RG time l_0, and defines a mass scale $\Lambda = a_0^{-1} e^{-l_0}$ that gives an estimate of the largest gap in the model (a_0^{-1} is a UV cutoff). At this point, we extract the values of all the $g_i(l_0)$ and draw them, renormalized by $g_1(l_0)$ $[g_i/g_1(l_0)]$ on the ring diagram. We reinitiate the couplings for a new θ and restart the procedure for all values of θ. The resulting diagram looks very similar for all $N > 2$ and different regimes can be defined (see Fig. 3 for $N = 3$) as a function of the lattice coupling constants U and V. Two qualitatively different behaviors of the flow can be identified in the asymptotic limit of weak coupling, where l_0 is large (small Ra_0). In regions (I) and (II) of Fig. 3, at large l_0, the ratios g_i/g_1 do not evolve anymore with the RG time and have already reached fixed values when the RG iterations are stopped. On the other hand, in region (III), g_1 is always the first coupling to reach the limit value G at which we stop the RG; the ratios $g_i/g_1(l_0)$ for $i = 3,4,5$ vanish in the weak coupling limit:

$$\lim_{R\to 0}[g_i/g_1(l_0)] = 0, \tag{32}$$

whereas the ratio $g_2/g_1(l_0)$ remains finite. This property will be important when we will derive effective models to describe

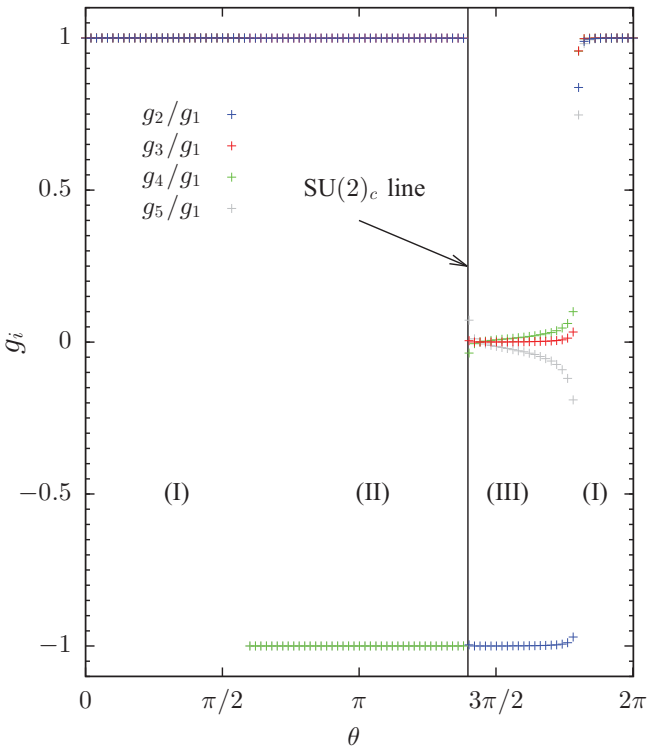

FIG. 3. (Color online) Ratio of the coupling constants, to which the RG flow leads in the IR limit, for $N = 3$; θ spans a ring with fixed radius $R = 0.1t$ in the phase diagram: $U = R\cos\theta$, $V = R\sin\theta$. Three different regions can be defined as function of θ.

this last region. We now turn to the description of the physical properties of the different regimes.

In the region (I) of Fig. 3, all coupling constants of the low-energy effective Hamiltonian (24) flow to strong coupling in the infrared (IR) limit at fixed ratio: $g_i/g_1 = 1$ $(i = 1, \ldots, 5)$. Along this special isotropic ray, model (24) displays an extended global SO($4N$) symmetry and becomes equivalent to the SO($4N$) Gross-Neveu (GN) model,[50] in the sense that the low-energy spectrum model of (24) is adiabatically connected to that of the SO($4N$) GN model (for a precise discussion, see Ref. 49). This phenomenon is an example of a dynamical symmetry enlargement by the interactions as found in half-filled two-leg Hubbard ladders or in the half-filled U(4) Hubbard chain, with the emergence of an SO(8) symmetry that becomes asymptotically exact in the weak-coupling limit.[37,51,52]

The SO($4N$) GN model is a massive integrable field theory whose mass spectrum is known exactly.[53,54] It consists of the elementary fermions with mass m, their bound states, and of kinks. The bound states have masses ($N > 1$)

$$m_n = m\,\frac{\sin\left(\frac{\pi n}{2(2N-1)}\right)}{\sin\left(\frac{\pi}{2(2N-1)}\right)}, \tag{33}$$

with $n = 2, \ldots, 2N-2$, while the kinks' mass reads

$$m_{\text{kinks}} = \frac{m}{2\sin\left(\frac{\pi}{2(2N-1)}\right)}. \tag{34}$$

The $N = 2$ case is special since the kinks' mass is equal to that of the fermions. The SO(8) GN model enjoys a

triality symmetry which has been exploited in the study of the half-filled two-leg Hubbard ladder.[51,55] In the $N > 2$ case, the lowest excitations are the fermions which transform into the vectorial representation of the SO($4N$) group: They have the same quantum numbers as the original fermions R_α, L_α and $R_\alpha^\dagger, L_\alpha^\dagger$.

The kinks transform in the spinorial representations of SO($4N$). It is more transparent to characterize these states by giving their charge and spin quantum numbers under U(1)$_c$ and SU($2N$) respectively: The kinks are those 2^{2N} states that carry charge $Q_k = k - N$ and transform in the ω_k representation of SU($2N$), where k varies from 0 to $2N$. One can distinguish even and odd kinks, which transform in the even (odd, respectively) spinorial representation and correspond to even (odd, respectively) k's. In particular, the low-energy spectrum of the SO($4N$) GN model contains Sp($2N$) spin-singlet states with charge $Q = \pm N$ which can be viewed as the generalization of the Cooperon excitations of the $N = 2$ case.[51,55] These kink states identify with those discussed in Sec. II A.

The development of the strong-coupling regime in the SO($4N$) GN model leads to the generation of a spectral gap and the formation of a SP phase for all $N > 1$ with order-parameter

$$\mathcal{O}_{\mathrm{SP}} = i(L_\alpha^\dagger R_\alpha - \mathrm{H.c.}). \tag{35}$$

This order parameter is the continuum limit of the spin Peierls operator $\mathcal{O}_{\mathrm{SP}} = (-1)^i \sum_\alpha c^\dagger_{\alpha,i+1} c_{\alpha,i}$ and it has a nonzero expectation value in the GS as can be seen by a direct semiclassical approach of the SO($4N$) GN model. The phase is twofold degenerate and breaks spontaneously the one-step translation symmetry (T_{a_0}): $L_\alpha \to -iL_\alpha, R_\alpha \to iR_\alpha$ since $\mathcal{O}_{\mathrm{SP}} \to -\mathcal{O}_{\mathrm{SP}}$ under T_{a_0}. This SP phase contains the U($2N$) line ($V = 0$) with $U > 0$, that is, the repulsive U($2N$) Hubbard model.

The second region of Fig. 3 can be easily determined with help of the duality symmetry Ω_1. The transformation of the SO($4N$) isotropic line under Ω_1 is $1 = g_2/g_1 = g_3/g_1 = -g_4/g_1 = -g_5/g_1$, which turns out to be the asymptote of the RG flow in the region (II) of Fig. 3. We thus deduce a second Mott-insulating phase which is obtained from the SP phase by applying the duality symmetry Ω_1. Since $L_\alpha \to iL_\alpha$ under Ω_1, its order parameter can be obtained from Eq. (35):

$$\mathcal{O}_{\mathrm{CDW}} = L_\alpha^\dagger R_\alpha + \mathrm{H.c.}, \tag{36}$$

which is nothing but the continuum limit of the $2k_F$ CDW operator: $\mathcal{O}_{\mathrm{CDW}} = \sum_\alpha (-1)^i c^\dagger_{\alpha,i} c_{\alpha,i}$. Region (II) is thus a fully gapped CDW phase. This CDW phase contains the U($2N$) line ($V = 0$) with $U < 0$.

What happens in region (III) of Fig. 3 is clearly of a different nature: The RG flow displays no symmetry enlargement, and we have to develop other tools to tackle the physics in this interesting region. This is done in the next section, where we reveal striking differences according to the parity of N. Before that, we would like to give hand-waving arguments, based on the spectrum of the SO($4N$) GN model, supporting this even-odd scenario. To understand what happens to the system when one leaves regions (I) and (II) where symmetry enlargement occurs, one should recast the whole particle content of the SO($4N$) GN model in multiplets of the internal continuous symmetry group of our problem, namely, Sp($2N$) $\times$ U(1)$_c$. One already knows how the SO($4N$) multiplets split into U(1)$_c$ $\times$ SU($2N$) representations, which we write (Q,λ) with λ an SU($2N$) weight and Q the U(1)$_c$ charge (the number of fermions measured with respect to the GS). Denoting the vectorial representation (to which the GN "fundamental fermions" belongs) by $\mathcal{V}$, the even spinorial (to which even kinks belong) by $S^{(+)}$ and the odd spinorial (to which odd kinks belong) by $S^{(-)}$, one has

$$\begin{aligned} \mathcal{V} &= (1,\omega_1) \oplus (-1,\omega_{2N-1}), \\ S^{(+)} &= \oplus_{k=0}^{N} (2k - N, \omega_{2k}), \\ S^{(-)} &= \oplus_{k=0}^{N-1} (2k + 1 - N, \omega_{2k+1}). \end{aligned} \tag{37}$$

A quick way to check those quantum numbers is to note that they must be compatible with the fundamental fermions being a bound state of two kinks. The only missing piece of information is the splitting of the SU($2N$) representations ω_k into Sp($2N$) representation. Denoting by $\bar{\omega}_k$ the kth Sp($2N$) fundamental representation, one has $\omega_{2n} = \oplus_{k=0}^{n} \bar{\omega}_{2k}$ and $\omega_{2n+1} = \oplus_{k=0}^{n} \bar{\omega}_{2k+1}$, so that any SU($2N$) representation ω_{2n} contains one and only one Sp($2N$) singlet, whereas all states of ω_{2n+1} carry nonzero Sp($2N$) spin.

Now one notices that region (III) of Fig. 3 occurs at negative V, where the system tends to favor Sp($2N$) singlets. Let us assume that there is adiabatic continuity in the low-energy part of the spectrum. Then, the quantum numbers of the lowest energy modes can be obtained by looking at those states in the SO($4N$) GN spectrum that are Sp($2N$) singlets. It results that when N is even, one expects the "elementary" charged particle [with the smallest U(1)$_c$ charge] to carry charge $Q = \pm 2$. On the other hand, when N is odd, there is a kink state that is a Sp($2N$) singlet *and* carries charge $Q = \pm 1$. We will shortly see that this even-odd dichotomy does indeed occur and that the elementary charged particles have the aforementioned charges.

D. Even-odd scenario

The last region of the RG flow of Fig. 3, that is, region (III), is difficult to analyze due to the absence of the second duality symmetry Ω_2 when $N > 2$. In this region, which includes the SU(2)$_c$ line with $V = NU$ and $U < 0$, the operator with coupling constant g_1 in the low-energy effective Hamiltonian (24) reaches the strong-coupling regime before the others. In the limit of weak coupling, one has a separation of energy scales, due to the property (32) of the RG flow. Neglecting all other couplings for the moment, the corresponding perturbation is an integrable massive field theory for $g_1 > 0$.[56,57] A spin gap Δ_s thus opens for the Sp($2N$) spin sector in region (III). The next step of the approach is to integrate out these spin degrees of freedom to derive an effective Hamiltonian in the low-energy limit $E \ll \Delta_s$ from which the physical properties of region (III) will be deduced.

1. Parafermionization

The resulting low-energy effective Hamiltonian involves the remaining degrees of freedom of the initial conformal embedding (19), that is, the SU(2)$_N$ sector. Since the global continuous symmetry of model (24) is, in general, U(1)$_c$ $\times$ Sp($2N$), we need to understand how we go from the

$SU(2)_N$ CFT to the $U(1)_c$ one. Such a mapping is realized by the conformal embedding: $\mathbb{Z}_N \sim SU(2)_N/U(1)_c$, which defines the $\mathbb{Z}_N$ parafermionic CFT series with central charge $c = 2(N-1)/(N+2)$.[58,59] This CFT describes the critical properties of 2D $\mathbb{Z}_N$ generalizations of the Ising model. The $\mathbb{Z}_N$ CFT is generated by the parafermionic currents $\Psi_{kL,R}$ $(k = 1, \ldots, N)$ with scaling dimensions $h_k = k(N-k)/N$.

The different operators of Eq. (24) can be written in this parafermionic basis. First of all, the $SU(2)_N$ currents (21) can be directly expressed in terms of $\Psi_{1L,R}$ and a bosonic field Φ_c which accounts for charge fluctuations:[58]

$$\begin{aligned} \mathcal{J}^{\dagger}_{L,R} &\simeq \frac{\sqrt{N}}{2\pi} : \exp(\pm i\sqrt{8\pi/N}\ \Phi_{cL,R}) : \Psi_{1L,R}, \\ \mathcal{J}^{z}_{L,R} &\simeq \sqrt{\frac{N}{2\pi}}\partial_x \Phi_{cL,R}, \end{aligned} \tag{38}$$

where the charge field $\Phi_c = \Phi_{cL} + \Phi_{cR}$ is a compactified bosonic field with radius $R_c = \sqrt{N/2\pi}$: $\Phi_c \sim \Phi_c + \sqrt{2\pi N}$. The remaining currents of Eq. (24) can also be expressed in terms of the parafermionic degrees of freedom using the results of Ref. 23:

$$\begin{aligned} J^i_L J^i_R &\sim \epsilon_1 \mathrm{Tr}\phi^{(2)}, \\ J^{i+}_L J^{i-}_R &\sim \mu_2 \mathrm{Tr}\phi^{(2)} \exp\left(i\sqrt{8\pi/N}\ \Phi_c\right), \end{aligned} \tag{39}$$

where $\phi^{(2)}$ is the second primary operator of the $Sp(2N)_1$ CFT with scaling dimension $2N/(N+2)$. In Eq. (39), ϵ_1 is the first thermal operator of the $\mathbb{Z}_N$ CFT with scaling dimension $4/(N+2)$, and μ_2 is the second disorder operator with scaling dimension $2(N-2)/N(N+2)$ which orders when the $\mathbb{Z}_N$ symmetry is not spontaneously broken.[58]

Before investigating the low-energy limit $E \ll \Delta_s$, it is crucial to analyze the hidden discrete symmetries of model (24) which become explicit thanks to the conformal embedding. It is well known that the $\mathbb{Z}_N$ CFT has a global $\mathbb{Z}_N \times \widetilde{\mathbb{Z}}_N$ discrete symmetry under which the parafermionic currents Ψ_{kL} (respectively, Ψ_{kR}) carry a (k,k) [respectively, $(k,-k)$] charge:[58]

$$\begin{aligned} \Psi_{kL,R} &\to e^{i2\pi mk/N}\Psi_{kL,R} \ \text{ under } \ \mathbb{Z}_N, \\ \Psi_{kL,R} &\to e^{\pm i2\pi mk/N}\Psi_{kL,R} \ \text{ under } \ \widetilde{\mathbb{Z}}_N, \end{aligned} \tag{40}$$

with $m = 0, \ldots, N-1$. The thermal operator ϵ_1 transforms as a singlet under these discrete symmetries while the order and disorder operators σ_k, μ_k carry, respectively, a $(k,0)$ and $(0,k)$ charge:

$$\begin{aligned} \sigma_k &\to e^{i2\pi mk/N}\sigma_k \ \text{ under } \ \mathbb{Z}_N, \\ \mu_k &\to e^{i2\pi mk/N}\mu_k \ \text{ under } \ \widetilde{\mathbb{Z}}_N, \end{aligned} \tag{41}$$

and σ_k (respectively, μ_k) remains unchanged under the $\widetilde{\mathbb{Z}}_N$ (respectively, $\mathbb{Z}_N$) symmetry. The $\mathbb{Z}_N$ symmetry of the parafermions has a simple interpretation in terms of the original lattice fermions or the Dirac fermions of the continuum limit. It is nothing but a special phase transformation $c_{\alpha,i} \to e^{-i\pi m/N}c_{\alpha,i}$ or, in the continuum description,

$$L_\alpha \to e^{-i\pi m/N}L_\alpha, \quad R_\alpha \to e^{-i\pi m/N}R_\alpha, \tag{42}$$

with $m = 0, \ldots, N-1$. This $\mathbb{Z}_N$ symmetry leaves invariant model (24), and the correspondences (38), (39) are also compatible with the definition (42). In contrast, the $\widetilde{\mathbb{Z}}_N$ symmetry of the parafermions does not exist on the lattice. Away from half filling, it becomes an independent emergent symmetry of the model in the continuum limit and takes the form[22,23]

$$L_\alpha \to e^{-i\pi m/N}L_\alpha, \quad R_\alpha \to e^{i\pi m/N}R_\alpha. \tag{43}$$

At half filling, this transformation is no longer a symmetry of model (24) due to the umklapp operators. The $\widetilde{\mathbb{Z}}_N$ symmetry has a more subtle role here: Its combination with the following identification on the charge bosonic field:

$$\Phi_c \sim \Phi_c - m\sqrt{\frac{2\pi}{N}} + p\sqrt{\frac{N\pi}{2}}, \quad m = 0, \ldots, N-1, \tag{44}$$

becomes a symmetry of model (24), as can be seen from Eq. (39). In fact, this symmetry is a gauge redundancy since it corresponds to the identity in terms of the Dirac fermions. The last important discrete symmetries of the problem are the Ω_1 duality transformation (31) and the one-step translation invariance (T_{a_0}), which only affect the charge field:

$$\begin{aligned} \Omega_1 &: \Phi_c \to \Phi_c + \frac{1}{2}\sqrt{\frac{N\pi}{2}}, \\ T_{a_0} &: \Phi_c \to \Phi_c + \sqrt{\frac{N\pi}{2}}. \end{aligned} \tag{45}$$

2. Low-energy Hamiltonian

We are now in position to derive the low-energy limit $E \ll \Delta_s$ by integrating out the gapful $Sp(2N)$ degrees of freedom. Using the parafermionization formulas (38, 39), one finds

$$\begin{aligned} \mathcal{H}_{\mathrm{int}} = \lambda_2\epsilon_1 &+ \lambda_3\partial_x\Phi_{cL}\partial_x\Phi_{cR} \\ &+ \frac{\lambda_4}{2}[\mu_2 \exp(i\sqrt{8\pi/N}\ \Phi_c) + \mathrm{H.c.}] \\ &+ \frac{\lambda_5}{2}[\Psi_{1L}\Psi^{\dagger}_{1R}\exp(i\sqrt{8\pi/N}\ \Phi_c) + \mathrm{H.c.}], \end{aligned} \tag{46}$$

where $\lambda_{2,4,5} \simeq \langle \mathrm{Tr}\phi^{(2)}\rangle g_{2,4,5}$ and $\lambda_3 = g_3 N/2\pi$. The low-energy Hamiltonian (46) enables us to explore the whole phase diagram of the model for all N. Along the $SU(2)_c$ line with $V = NU$, model (46) can be written in terms of the $SU(2)_N$ fields:

$$\mathcal{H}_{\mathrm{int}} = g_3\vec{\mathcal{J}}_R \cdot \vec{\mathcal{J}}_L + \lambda_2 \mathrm{Tr}\Phi^{(1)}, \tag{47}$$

where $\Phi^{(1)}$ is the spin-1 primary field of the $SU(2)_N$ CFT with scaling dimension $4/(N+2)$. The effective Hamiltonian (47) is the low-energy theory of the spin-$N/2$ SU(2) Heisenberg chain derived by Affleck and Haldane in Ref. 60. As shown by these authors, model (47) has a spectral gap, when N is even, while it describes a massless flow to the $SU(2)_1$ CFT when N is odd, in full agreement with Haldane's conjecture.[60] The latter result has also been found by means of a parafermionic approach similar to Eq. (46) in the presence of an SU(2) symmetry.[61]

The crucial point to map out the general phase diagram of the low-energy Hamiltonian (46) for all N stems from the status of the $\mathbb{Z}_N$ symmetry (42). The first term in Eq. (46)

describes an integrable deformation of the $\mathbb{Z}_N$ CFT which is always a massive field theory for all signs of λ_2.[62] In our conventions, if $\lambda_2 > 0$ (respectively, $\lambda_2 < 0$) the $\mathbb{Z}_N$ symmetry is unbroken (respectively, spontaneously broken) and the disorder fields (respectively, order fields) condense, $\langle \mu_k \rangle \neq 0$ (respectively $\langle \sigma_k \rangle \neq 0$) for all $k = 1, \ldots, N$.

Let us first reinvestigate the emergence of the CDW, SP phases in regions (I, II) within this parafermionization approach. When $\lambda_2 > 0$ (i.e., $g_2 > 0$), the $\mathbb{Z}_N$ symmetry remains unbroken and one may integrate out the gapful parafermionic degrees of freedom to derive an effective field theory on the charge bosonic field. Since we have $\langle \mu_2 \rangle \neq 0$ and $\langle \Psi_{1L} \Psi_{1R}^\dagger \rangle \neq 0$ in the $\mathbb{Z}_N$ high-temperature phase, we obtain from Eq. (46)

$$\mathcal{H}_c = \frac{v_c}{2} \left(\frac{1}{K_c} (\partial_x \Phi_c)^2 + K_c (\partial_x \Theta_c)^2 \right) + g_c \cos(\sqrt{8\pi/N}\ \Phi_c), \tag{48}$$

where the Luttinger parameter is given by

$$K_c = \frac{1}{\sqrt{1 + g_3 N/(2\pi v_F)}}. \tag{49}$$

The low-energy Hamiltonian for the charge degrees of freedom (48) is the well-known sine-Gordon model at $\beta^2 = 8\pi K_c/N$. We thus deduce the existence of a charge gap when $K_c < N$, which is always the case at weak coupling as seen from Eq. (49). The nature of the Mott-insulating phase depends on the sign of g_c, which is changed by the duality transformation Ω_1 (45). When $g_c < 0$ (i.e., $g_4 < 0$), the development of the strong-coupling regime of the sine-Gordon model (48) is accompanied by the pinning of the charged field on the minima: $\langle \Phi_c \rangle = p\sqrt{N\pi/2}$, p being an integer. Since we have the identification $\Phi_c \sim \Phi_c + \sqrt{2\pi N}$ due to the periodicity of the charge field, we deduce that the insulating phase is twofold degenerate with minima: $\langle \Phi_c \rangle = 0$ and $\langle \Phi_c \rangle = \sqrt{N\pi/2}$; that is, the one-step translation symmetry (45) is spontaneously broken. The low-lying excitations are massive kinks and antikinks which interpolate between the two GS. The charges associated to these excitations are

$$Q = \pm\sqrt{2N/\pi} \int dx\ \partial_x \Phi_c = \pm N. \tag{50}$$

For $N = 2$, the excitations correspond to the Cooperon excitations of the half-filled two-leg Hubbard ladder.[51] The charge excitations (50) correspond to the generalization of these Cooperons. That they are the charge excitations with the minimal charge can be deduced from considerations on symmetry: Among the spectrum of the SO($4N$) GN model, they are the only charged states that are both Sp($2N$) singlets and neutral under $\mathbb{Z}_N$. [Indeed, the $\mathbb{Z}_N$ charge of any state can be simply read off from the way it transforms under SU($2N$): States in ω_k carry a $\mathbb{Z}_N$ charge given by k mod N.] The physical nature of the twofold degenerate Mott-insulating phases can be determined by expressing the SP and CDW order parameters (35, 36)in terms of the charge and the $\mathbb{Z}_N$ fields:[23]

$$L_\alpha^\dagger R_\alpha \sim \exp(i\sqrt{2\pi/N}\ \Phi_c)\mu_1 \mathrm{Tr}\ \phi^{(1)}, \tag{51}$$

where $\phi^{(1)}$ is the first Sp$(2N)_1$ primary field with scaling dimension $(2N+1)/2(N+2)$. Averaging over the Sp($2N$) and $\mathbb{Z}_N$ degrees of freedom, we obtain

$$\begin{aligned} \mathcal{O}_{\mathrm{CDW}} &\sim \cos(\sqrt{2\pi/N}\ \Phi_c), \\ \mathcal{O}_{\mathrm{SP}} &\sim \sin(\sqrt{2\pi/N}\ \Phi_c). \end{aligned} \tag{52}$$

The phase with $g_c < 0$ (i.e., $g_4 < 0$) is thus a CDW phase ($\langle \mathcal{O}_{\mathrm{CDW}} \rangle \neq 0$) and corresponds to the region (II) of Fig. 3. The second phase with $g_c > 0$ is obtained from the CDW phase by the application of the duality transformation Ω_1. The pinnings of the charge field are then $\langle \Phi_c \rangle = \sqrt{N\pi/8}$ and $\langle \Phi_c \rangle = 3\sqrt{N\pi/8}$, which signals the formation of a SP phase in the region (I) of Fig. 3 since from Eq. (52), $\langle \mathcal{O}_{\mathrm{SP}} \rangle \neq 0$. The quantum phase transition between the CDW/SP phases belongs to the self-dual manifold of the duality symmetry Ω_1. Using the definition (45), one finds that the low-energy Hamiltonian of the transition is given by

$$\begin{aligned} \mathcal{H}_{\mathrm{selfdual}} = \frac{v_c}{2} &\left(\frac{1}{K_c} (\partial_x \Phi_c)^2 + K_c (\partial_x \Theta_c)^2 \right) \\ &+ g_c \cos(\sqrt{32\pi/N}\ \Phi_c). \end{aligned} \tag{53}$$

The resulting quantum phase transition is of BKT type. The transition displays a quantum-critical behavior with one gapless bosonic mode if $K_c > N/4$. At this point, we need complementary numerical techniques to extract the value of K_c in order to conclude on the nature of the transition.

Finally, the case with $\lambda_2 < 0$ (or $g_2 < 0$) corresponds to region (III) of Fig. 3 where the $\mathbb{Z}_N$ symmetry is now spontaneously broken. In this $\mathbb{Z}_N$ low-temperature phase, the $\mathbb{Z}_N$ degrees of freedom are still fully gapped and the disorder operators now average to zero: $\langle \mu_k \rangle = 0$. Similarly to the $\lambda_2 > 0$ case, we can integrate out the parafermionic fields to obtain an effective field theory on the charge bosonic field. However, due to the presence of the μ_2 operator in Eq. (46), the resulting integration strongly depends on the parity of N.

3. *Phase diagram in the N odd case (N > 1)*

Let us first consider the case where N is odd. Since all the parafermionic operators in Eq. (46) average to zero in the $\mathbb{Z}_N$ broken phase, one has to consider higher orders in perturbation theory to derive an effective theory for the charge field. The $\mathbb{Z}_N$ fields of model (46) carry a charge 2 under the $\widetilde{\mathbb{Z}}_N$ symmetry [see Eq. (41) with $k = 2$ for μ_2]. When N is odd, one has to use the Nth order of perturbation theory to cancel out the $\widetilde{\mathbb{Z}}_N$ charge of μ_2 so that we find

$$\begin{aligned} \mathcal{H}_c^{\mathrm{odd}} = \frac{v_c}{2} &\left(\frac{1}{K_c} (\partial_x \Phi_c)^2 + K_c (\partial_x \Theta_c)^2 \right) \\ &+ g_c \cos(\sqrt{8\pi N}\ \Phi_c), \end{aligned} \tag{54}$$

with $g_c \sim g_4^N$, while we do not have any estimate of the Luttinger parameter except the bare one (49). On symmetry grounds, the effective Hamiltonian (54) can also be derived by finding the vertex operator in the charge sector with the smallest scaling dimension which is compatible with translational invariance (45) and the redundancy (44). The resulting low-energy Hamiltonian (54) takes the form of a sine-Gordon model at $\beta^2 = 8\pi N K_c$ so that a charge gap opens

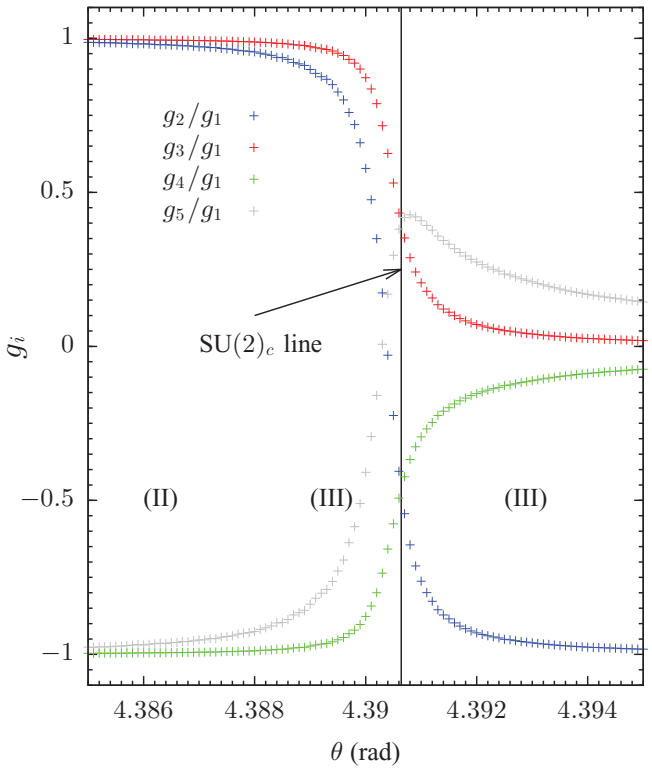

FIG. 4. (Color online) Values of the coupling constants g_i in the infrared limit, in the vicinity of the transition from CDW phase (II) to BCS critical phase (III), close to the SU(2)$_c$ symmetric line ($V = NU$). Notations are the same as in Fig. 3.

when $K_c < 1/N$. For $K_c = 1/N$, this sine-Gordon model displays a hidden SU(2) symmetry which should correspond to the SU(2)$_c$ line $V = NU$ with $U < 0$ that belongs to region (III). Close to this SU(2)$_c$ line, the RG flow of Fig. 4 shows that the coupling constant g_4 is negative so that $g_c < 0$. When $K_c < 1/N$, the charge bosonic field is thus pinned on the minima: $\langle\Phi_c\rangle = p\sqrt{\pi/2N}$, p being an integer. Taking into account the gauge redundancy (44), we find that the strong-coupling phase of the sine-Gordon model (54) is twofold degenerate with $\langle\Phi_c\rangle = 0$ and $\langle\Phi_c\rangle = \sqrt{\pi/2N}$. The charges of the massive kinks and antikinks excitations are now

$$Q = \pm\sqrt{2N/\pi}\int dx\ \partial_x\Phi_c = \pm 1, \tag{55}$$

in sharp contrast to the charge $Q = \pm N$ of excitations (50) of the CDW phase of region (II). At this point, we need to find a local order parameter to fully characterize the twofold degenerate Mott insulating phase in region (III). When the Sp($2N$) and $\mathbb{Z}_N$ degrees of freedom are integrated out, the expression of the bilinear Dirac fermions (51) is naively short-ranged in region (III), since it contains the first disorder parameter. However, by fusing this operator with the Hamiltonian (46) at the $(N-1)/2$th order of perturbation theory, the disorder operator cancels out and one obtains the following low-energy description:

$$L_\alpha^\dagger R_\alpha \sim \exp(i\sqrt{2\pi N}\ \Phi_c). \tag{56}$$

In region (III), where the $\mathbb{Z}_N$ is spontaneously broken, the CDW and SP operators then read as follows:

$$\begin{aligned}\mathcal{O}_{\rm CDW} &\sim \cos(\sqrt{2\pi N}\ \Phi_c),\\ \mathcal{O}_{\rm SP} &\sim \sin(\sqrt{2\pi N}\ \Phi_c),\end{aligned} \tag{57}$$

so that $\langle\mathcal{O}_{\rm CDW}\rangle \neq 0$. The insulating phase in region (III) when $K_c < 1/N$ is thus the continuation of the CDW phase of region (II). However, there is a striking difference at the level of the low-lying excitations: The generalization of the Cooperon excitations with charge $Q = N$ is no longer a stable excitation in region (III) but becomes a diffusive state made of the kinks (55) which are massive holons. The situation is very similar to the SP phase of the half-filled U(4) Hubbard model between the weak and strong coupling regimes.[37] As far as the GS properties are concerned, there is a smooth crossover when the $\mathbb{Z}_N$ symmetry changes its status at $\lambda_2 = 0$ and not a $\mathbb{Z}_N$ quantum phase transition as is the case away from half filling.[22,23]

When $K_c > 1/N$, the charge degrees of freedom become gapless. We then need to determine the leading instability of this phase, that is, the one that has the slowest decaying correlation functions. The singlet-pairing operator can be expressed in terms of the charge and the $\mathbb{Z}_N$ fields as[23]

$$P_{00}^\dagger \sim \exp(i\sqrt{2\pi/N}\ \Theta_c)\sigma_1 \mathrm{Tr}\,\phi^{(1)}. \tag{58}$$

Since the $\mathbb{Z}_N$ symmetry is broken, we have $\langle\sigma_1\rangle \neq 0$ and the low-energy representation of the singlet-pairing operator is thus $P_{00}^\dagger \sim \exp(i\sqrt{2\pi/N}\ \Theta_c)$. The gapless phase stems from the competition of this singlet-pairing operator, which cannot condense, and the CDW operator (57). The leading asymptotics of their equal-time correlation functions can then be straightforwardly determined:

$$\begin{aligned}\langle P_{00}^\dagger(x)P_{00}(0)\rangle &\sim A\ x^{-1/NK_c},\\ \langle n(x)n(0)\rangle &\sim -\frac{NK_c}{\pi^2x^2} + (-1)^{x/a_0}B\ x^{-NK_c},\end{aligned} \tag{59}$$

where $n(x)$ is the continuum limit of the lattice density operator n_i, and A, B are nonuniversal amplitudes. Since $K_c > 1/N$, the leading instability of this gapless phase is the BCS singlet-pairing.

The quantum phase transition between the gapful CDW phase and the gapless BCS phase occurs at $K_c = 1/N$, which corresponds to the SU(2)$_c$ ($V = NU < 0$) line. On this line, we observe that the exponents of the correlation functions of Eq. (59) are identical. Using the pseudospin operator (11), we deduce the following leading asymptotics from Eq. (59):

$$\begin{aligned}\langle\mathcal{S}^\dagger(x)\mathcal{S}^-(0)\rangle &\sim x^{-1},\\ \langle\mathcal{S}^z(x)\mathcal{S}^z(0)\rangle &\sim (-1)^{x/a_0}\ x^{-1}.\end{aligned} \tag{60}$$

The model with $K_c = 1/N$ displays a quantum critical behavior with central charge $c = 1$ for all odd N and corresponds to the SU(2)$_1$ universality class. This result is in perfect agreement with the strong-coupling analysis of Sec. II along the SU(2)$_c$ line, where the pseudospin operator (11) is a spin-$N/2$, that is, half-integer, operator. The low-energy properties of SU(2) half-integer Heisenberg spin chains are indeed known to be governed by the SU(2)$_1$ CFT.[60] In the spin language, the

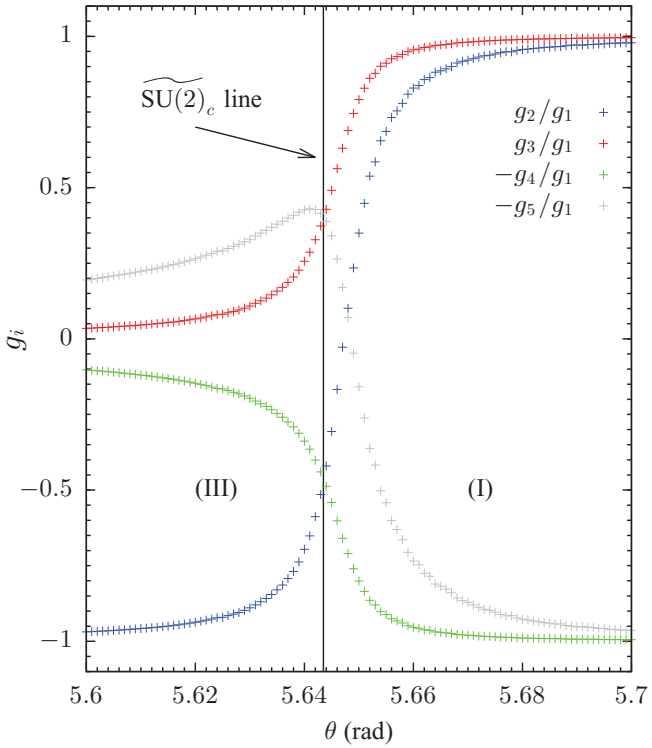

FIG. 5. (Color online) Values of the coupling constants g_i in the IR limit, in the vicinity of the transition between the BCS (III) and SP (I) phases, displaying the restoration of an SU(2) symmetry, denoted $\widetilde{SU(2)}_c$, which is the dual of the lattice $SU(2)_c$ symmetry ($V = NU$): $g_2 = -g_4$ and $g_3 = -g_5$. We use the same notations as in Fig. 3.

CDW and BCS phases are, respectively, the analog of the Ising and XY phases and the quantum phase transition occurs at the SU(2) Heisenberg point.

When we deviate from the $SU(2)_c$ line in the gapless BCS phase, Figs. 4 and 5 show that g_3 decreases and then increases as a function of the interaction. Using the naive estimate of the Luttinger parameter (49), we deduce that K_c increases from $K_c = 1/N$ at the $SU(2)_c$ line and then decreases until one reaches the SP phase of region (I). The resulting transition and its properties can be deduced from the CDW/BCS transition by the duality symmetry Ω_1. Indeed, under the transformation (45), the sign of g_c of model (54) is changed and the gapful insulating phase when $K_c < 1/N$ is twofold degenerate with $\langle\Phi_c\rangle = \sqrt{\pi/8N}$ and $\langle\Phi_c\rangle = 3\sqrt{\pi/8N}$. The SP order parameter (57) acquires a nonzero expectation value in this phase: $\langle\mathcal{O}_{SP}\rangle \neq 0$. As far as the GS properties are concerned, this phase is the continuation of the SP phase of region (I). The quantum phase transition between the BCS and SP phases occurs at $K_c = 1/N$. Its position corresponds to an SU(2) line with $g_2 = -g_4$ and $g_3 = -g_5$, which is obtained from the lattice $SU(2)_c$ line $V = NU < 0$ ($g_2 = g_4$, $g_3 = g_5$) by the application of the duality symmetry Ω_1. The resulting SU(2) line, noted $\widetilde{SU(2)}_c$ in Fig. 5, does not exist on the lattice: It is an emergent SU(2) symmetry of the continuum limit.

As a summary, Fig. 6 shows the zero-temperature phase diagram of model (2) in terms of the lattice parameters U, V in the N odd case ($N > 1$), which results from the low-energy approach.

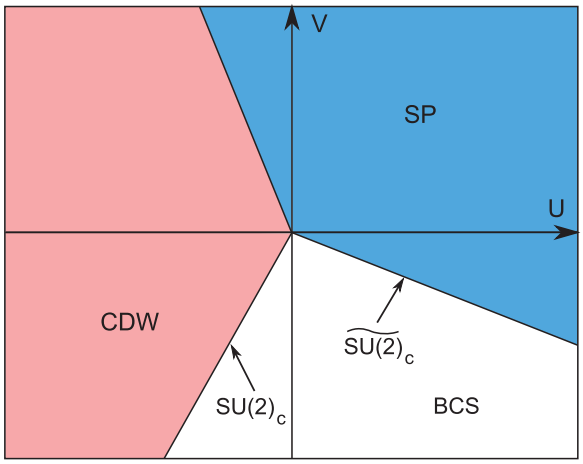

FIG. 6. (Color online) Phase diagram obtained by the low-energy approach in the N odd case ($N > 1$).

4. *Phase diagram in the N even case (N > 2)*

As in the N odd case, one has to consider higher orders in perturbation theory to derive an effective theory for the charge field Φ_c since all the parafermionic operators in Eq. (46) average to zero in the $\mathbb{Z}_N$ broken phase. When N is even, one needs the $N/2$th order of perturbation theory to cancel out the $\widetilde{\mathbb{Z}}_N$ charge of μ_2. The resulting low-energy Hamiltonian then reads as follows:

$$\mathcal{H}_c^{\text{even}} = \frac{v_c}{2}\left(\frac{1}{K_c}(\partial_x\Phi_c)^2 + K_c(\partial_x\Theta_c)^2\right) + g_c\cos(\sqrt{2\pi N}\,\Phi_c). \tag{61}$$

Alternatively, the effective Hamiltonian (61) can also be obtained by considering the vertex operator in the charge sector with the smallest scaling dimension which is compatible with translational invariance (45) and the gauge redundancy (44). The resulting low-energy Hamiltonian (61) takes the form of a sine-Gordon model at $\beta^2 = 2\pi N K_c$ so that a charge gap opens when $K_c < 4/N$. One sees that, right on the $SU(2)_c$ line where the Luttinger exponent is constrained ($K_c = 1/N$), the sine-Gordon parameter takes the special value $\sqrt{2\pi}$, at which it is known that a hidden SU(2) symmetry emerges.[63] The lowest energy modes are a massive triplet, the magnon of the integer spin Heisenberg model. Turning back to the generic situation $K_c < 4/N$ where a charge gap opens, the charge bosonic field is pinned into the following configurations:

$$\begin{aligned}\langle\Phi_c\rangle &= p\sqrt{\frac{2\pi}{N}}, && \text{if} \quad g_c < 0,\\ \langle\Phi_c\rangle &= \sqrt{\frac{\pi}{2N}} + p\sqrt{\frac{2\pi}{N}}, && \text{if} \quad g_c > 0,\end{aligned} \tag{62}$$

p being an integer. The lowest massive excitations are the soliton and antisoliton of the sine-Gordon model; they carry charge

$$Q = \pm\sqrt{2N/\pi}\int dx\ \partial_x\Phi_c = \pm 2, \tag{63}$$

which correspond to the Cooperon excitations. Using the gauge redundancy (44), we find that, in sharp contrast to the

CDW and SP phases, the insulating phase when $K_c < 4/N$ is nondegenerate, its GS being

$$\begin{aligned} \langle \Phi_c \rangle &= 0, \qquad \text{if} \quad g_c < 0, \\ \langle \Phi_c \rangle &= \sqrt{\frac{\pi}{2N}}, \qquad \text{if} \quad g_c > 0. \end{aligned} \tag{64}$$

Starting from the CDW phase of region (II), where the $\mathbb{Z}_N$ symmetry is unbroken, there is necessarily a quantum phase transition to the nondegenerate Mott-insulating phase of region (III) with broken $\mathbb{Z}_N$ symmetry. In particular, the disorder parameter μ_1 of Eq. (51) cannot be compensated using higher orders of perturbation theory as was the case for odd N. It means that in region (III), $\langle \mathcal{O}_{\rm CDW} \rangle = \langle \mathcal{O}_{\rm SP} \rangle = 0$ when the Sp($2N$) and $\mathbb{Z}_N$ degrees freedom are integrated out. It is natural to expect that the nondegenerate insulating phases, described by the pinning (64), signal the emergence of the HI and RS phases that we have identified in the strong-coupling approach (15). At this point, it is worth observing that the duality symmetry Ω_1 plays a subtle role in the even N case. Indeed, under the transformation (45), the cosine term of Eq. (61) transforms as

$$\cos(\sqrt{2\pi N}\ \Phi_c) \to (-1)^{N/2} \cos(\sqrt{2\pi N}\ \Phi_c), \tag{65}$$

so that there is room for an interesting $N/2$ even-odd effect.

$N/2$ even case. Let us first consider the $N/2$ even case. A naive estimate of the coupling constant g_c in higher orders of perturbation theory gives $g_c \sim -g_4^{N/2}$. The RG flow close to the SU(2)$_c$ line ($V = NU < 0$) in the $N/2$ even case is similar to the one in Fig. 4. In this region, we have $g_4 < 0$ so that the nondegenerate gapful phase is described by the locking $\langle \Phi_c \rangle = 0$ of Eq. (64). As seen in Fig. 4, this region contains the SU(2)$_c$ line where the strong-coupling analysis (15) predicts the emergence of the spin-$N/2$, that is, even spin, SU(2) Heisenberg chain. The low-lying excitation of the resulting Haldane phase is a gapped triplet state. From the expression of the pseudospin operator (11), one observes that it corresponds to a Cooperon excitation in full agreement with the prediction (63). We thus conclude that the Mott-insulating phase in the vicinity of the SU(2)$_c$ line ($V = NU < 0$), which is described by the sine-Gordon model (61) with $\langle \Phi_c \rangle = 0$, is the HI phase.

The topological order of the Haldane phase with integer spin $S = N/2 > 1$ has been less understood than the $S = 1$ case. This phase displays edge states with localized spin $N/4$ when OBC are used.[31] Unfortunately, we are not able to describe these boundary edge excitations by means of our low-energy approach except when $N = 2$.[15,40,64] On top of these end-chain states, the higher integer-spin Haldane phase should exhibit a nonlocal string ordering.[65–71] A very naive guess is to use the generalization of the string-order parameter (28) with spin-$N/2$ operator. In the low-energy limit, we find for $N/2$ even

$$\begin{aligned} &\lim_{|i-j|\to\infty} \left\langle \mathcal{S}_i^z e^{i\pi \sum_{k=i+1}^{j-1} \mathcal{S}_k^z} \mathcal{S}_j^z \right\rangle \\ &\quad \simeq \lim_{|x-y|\to\infty} \langle \sin(\sqrt{N\pi/2}\ \Phi_c(x)) \sin(\sqrt{N\pi/2}\ \Phi_c(y)) \rangle \\ &\quad = 0, \end{aligned} \tag{66}$$

since the HI phase is described by the pinning $\langle \Phi_c \rangle = 0$. This result is in full agreement with what is known at the Affleck, Kennedy, Lieb, Tasaki (AKLT) point[72] of the integer-spin Heisenberg chain,[65,66] and also from DMRG studies of the spin-2 Heisenberg chain.[67–71] A simple nonzero string order parameter in the HI phase, which we can estimate within our low-energy approach, is

$$\begin{aligned} &\lim_{|i-j|\to\infty} \left\langle \cos\left(\pi \sum_{k<i} \mathcal{S}_k^z\right) \cos\left(\pi \sum_{k<j} \mathcal{S}_k^z\right) \right\rangle \\ &\quad \simeq \lim_{|x-y|\to\infty} \langle \cos(\sqrt{N\pi/2}\ \Phi_c(x)) \cos(\sqrt{N\pi/2}\ \Phi_c(y)) \rangle \\ &\quad \neq 0. \end{aligned} \tag{67}$$

This lattice order parameter turns out to be nonzero at the AKLT point of even-spin Heisenberg chains.[73]

In summary, when $N/2$ is even, the HI phase is described at low-energy by the sine-Gordon model (61) with $K_c < 4/N$ and a nondegenerate GS $\langle \Phi_c \rangle = 0$. The quantum phase transition between the CDW and HI phases is difficult to determine exactly. On general grounds, we expect an Ising quantum phase transition or a first-order one due to the difference of the GS degeneracies between the two phases. In the CDW and HI phases, the charge bosonic field is locked at $\langle \Phi_c \rangle = 0$ so that the CDW/HI quantum phase transition is governed by the $\mathbb{Z}_N$ interacting field theory:

$$\mathcal{H}_{\rm int}^{\mathbb{Z}_N} = \lambda_2\ \epsilon_1 + \lambda_4 (\mu_2 + \text{H.c.}). \tag{68}$$

Model (68) is a deformation of the $\mathbb{Z}_N$ CFT perturbed by two relevant operators with scaling dimensions $4/(N+2)$ and $2(N-2)/N(N+2)$, respectively. When acting separately, each perturbation yields a massive field theory, but the interplay between them may give rise to a second-order phase transition at intermediate coupling. In this respect, when $\lambda_2 < 0$, the first operator in Eq. (68) orders the $\mathbb{Z}_N$ degrees of freedom while the second one wants to disorder them. We conjecture that this competition for $\lambda_2 < 0$ leads to a massless flow to a $\mathbb{Z}_2$ quantum critical point in the IR limit. The quantum phase transition between the CDW and HI phases thus belongs to the 2D Ising universality class with central charge $c = 1/2$. In the simplest $N = 4$ case, we can show this result explicitly by exploiting the fact that the $\mathbb{Z}_4$ parafermionic CFT has central charge $c = 1$ and so it should be possible to realize it with a single free Bose field. In fact, the correct identification is quite subtle and the $\mathbb{Z}_4$ CFT turns out to be equivalent to a Bose field living on the orbifold line at radius $R = \sqrt{3/2\pi}$.[74] However, as shown in the Appendix of Ref. 75, it is still possible to bosonize some fields of the $\mathbb{Z}_4$ CFT with a simple (periodic) Bose field Φ defined on the circle with radius $R = \sqrt{3/2\pi}$: $\Phi \sim \Phi + 2\pi R$. In this respect, the two operators of Eq. (68), with scaling dimension $2/3$ and $1/6$, take the form of vertex operators. The bosonized description of the effective field theory (68) reads

$$\mathcal{H}_{\rm int}^{\mathbb{Z}_4} = \lambda_2\ \cos(\sqrt{8\pi/3}\ \Phi) + \lambda_4 \sin(\sqrt{2\pi/3}\ \Phi). \tag{69}$$

This model is the so-called two-frequency sine-Gordon model which, for instance, governs the transition from a band insulator to a Mott insulator in the 1D ionic Hubbard model.[76] When $\lambda_2 < 0$ and for all signs of λ_4, model (69) displays a $\mathbb{Z}_2$ quantum critical point in the IR limit which has been analyzed

nonperturbatively in Refs. 76–78. We thus deduce that the quantum phase transition between the CDW and HI phases for $N = 4$ belongs to the 2D Ising universality class.

Let us now investigate the fate of the HI phase as one deviates from the $SU(2)_c$ line. As in the N odd case, there is a regime in region (III), away from the $SU(2)_c$ line, where the coupling g_3 that appears in the Luttinger parameter expression (49) decreases and then increases as function of the interaction (see Figs. 4 and 5). In the vicinity of the minimum of g_3, we expect the emergence of a gapless phase associated to the sine-Gordon model (61) with $K_c > 4/N$. The existence of this intermediate gapless phase will be confirmed numerically in Sec. VI by means of DMRG calculations. In this respect, the $N = 2$ case is very special since this phase shrinks to a line which marks the phase transition between HI and RS phases (see Fig. 2). This critical phase has only one gapless charge mode and the singlet-pairing has the same low-energy behavior as in the N odd case: $P_{00}^{\dagger} \sim \exp(i\sqrt{2\pi/N}\,\Theta_c)$. However, this phase is different from the gapless BCS phase of the N odd case. Indeed, as already stressed, the disorder parameter μ_1 of Eq. (51) cannot be compensated using higher orders of perturbation theory which means that the alternating part of the CDW operator is short ranged. We then deduce the following leading asymptotics of the equal-time correlation functions:

$$\begin{aligned} \langle P_{00}^{\dagger}(x) P_{00}(0)\rangle &\sim x^{-1/NK_c}, \\ \langle n(x)n(0)\rangle &\sim -\frac{NK_c}{\pi^2 x^2}, \end{aligned} \tag{70}$$

where in the density correlator, only the uniform part has a power-law decay. The leading instability is the singlet-pairing one when $K_c > 4/N$. The main difference with the gapless BCS phase of Fig. 6 stems from the fact that the alternating part of the density correlator (70) has now an exponential decay. The quantum phase transition between HI and BCS phases belongs to the BKT universality class.

The last regime of region (III), which corresponds to the transition between (III) and (I) of Fig. 5, can be identified by means of the duality symmetry Ω_1. Under this transformation (45), the CDW phase is changed into the SP phase. In contrast, from Eq. (65), we deduce that the sine-Gordon operator of the low-energy Hamiltonian (61) remains invariant when $N/2$ is even. The Mott-insulating phase in the vicinity of the $\widetilde{SU(2)}_c$ line of Fig. 5 is thus described by the strong-coupling regime of the sine-Gordon model (61) with $K_c < 4/N$ and the pinning $\langle\Phi_c\rangle = 0$. This phase is expected to be the RS phase, that is, the so-called large D phase of the integer spin Heisenberg chain,[45] which appears in the strong-coupling approach (15) for a sufficiently strong positive D. Interestingly enough, within our low-energy approach, this phase is described exactly in the same way as the HI phase. Thus, the two phases necessarily share the same order parameters, such as the string orders (66, 67). However, they should have different edge states but we could not, very unfortunately, investigate these boundary end excitations in our CFT approach. Recently, it has been argued that the edge-state structure of the even-spin Heisenberg chain is not protected by symmetry, in contrast to the odd case.[33] In particular, the authors of Ref. 33 have conjectured that there is an adiabatic continuity between the Haldane and large D phases in the even-spin case. The Haldane phase is thus equivalent to a topologically trivial insulating phase in this case. This adiabatic continuity has been shown numerically in the spin-2 XXZ Heisenberg chain with a single-ion anisotropy by finding a path where the two phases are connected without any phase transition.[34] In our problem, the HI and RS phases are separated by an intermediate gapless BCS phase. However, within our low-energy approach, the two nondegenerate Mott-insulating phases are described in the same manner by the sine-Gordon model (61) with $K_c < 4/N$ and the pinning $\langle\Phi_c\rangle = 0$. In this respect, our results strongly support the conjecture put forward in Ref. 33.

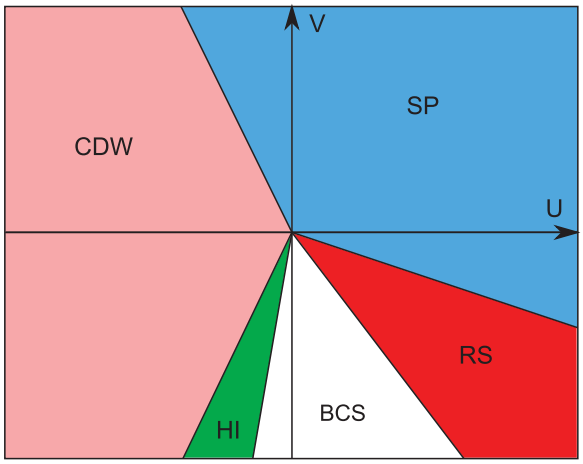

FIG. 7. (Color online) Phase diagram obtained by the low-energy approach in the N even case ($N > 2$).

Finally, the quantum phase transition between RS and SP phases is obtained from the effective theory (68) by the application of the duality symmetry Ω_1. The latter transformation changes the sign of the coupling constant λ_4 of the μ_2 operator. However, this sign is irrelevant for the competition between the two relevant operators in model (68). We thus expect that the resulting quantum phase transition still belongs to the 2D Ising universality class. In summary, Fig. 7 presents the phase diagram, in terms of the lattice parameters U, V in the $N/2$ even case.

$N/2$ odd case. The last case to consider is the case where $N/2$ is odd. In region (III), in the vicinity of the $SU(2)_c$ line, the charge bosonic field Φ_c of the sine-Gordon model (61) with $K_c < 4/N$ is now pinned at $\langle\Phi_c\rangle = \sqrt{\pi/2N}$ since $g_c > 0$. The nondegenerate Mott-insulating phase is the HI phase. This phase can be described by the generalization of the string-order parameter (28) with spin-$N/2$ operator. Indeed, in the low-energy limit and for the $N/2$ odd case, we find

$$\begin{aligned} &\lim_{|i-j|\to\infty} \left\langle \mathcal{S}_i^z e^{i\pi \sum_{k=i+1}^{j-1} \mathcal{S}_k^z} \mathcal{S}_j^z \right\rangle \\ &\quad \simeq \lim_{|x-y|\to\infty} \langle \sin\left(\sqrt{N\pi/2}\;\Phi_c(x)\right) \sin\left(\sqrt{N\pi/2}\;\Phi_c(y)\right)\rangle \\ &\quad \neq 0\,, \end{aligned} \tag{71}$$

in sharp contrast to the result (66) of the $N/2$ even case. For general odd-spin Heisenberg chain, the order parameter (71) is known to be nonzero contrarily to the even-spin case.[65,66] In this respect, there is thus a clear dichotomy in the HI phase, depending on the parity of $N/2$. For odd-spin Heisenberg chains, the authors of Ref. 33 have predicted that the Haldane

phase displays a topological order and is not equivalent to the large D phase as in the even-spin case. This scenario is in perfect agreement with our low-energy approach. Indeed, according to Eq. (65), the duality symmetry Ω_1 changes the sign of the vertex operator of model (61) when $N/2$ is odd. The physical properties of the RS phase are thus governed by the sine-Gordon model (61) with $K_c < 4/N$ and the pinning $\langle \Phi_c \rangle = 0$. In the $N/2$ odd case, the HI and RS phases are described by two different lockings of the charge bosonic field, in sharp contrast to the $N/2$ even case. In particular, the RS phase is described by the string-order parameter (67) and not (71), as the HI phase is. The HI and RS phases are thus totally distinct phases that cannot be adiabatically connected.

Finally, as in the $N/2$ even case, the transition between these two nondegenerate phases is accompanied by the formation of an intermediate gapless BCS phase with the properties (70). Unfortunately, in the $N/2$ odd case, we do not have access to a theory of the quantum phase transition between the CDW (respectively, SP) phase and the HI (respectively, RS) phase. We suspect, as in the $N/2$ even case, that the transition belongs to the 2D Ising universality class, but it certainly requires a proof. Figure 7 presents the phase diagram in the $N/2$ odd case which, apart from the subtleties on the topological nature of the HI phases, is identical to the $N/2$ even case. Last, we would like to emphasize that the $N = 2$ case (see Fig. 2) is not representative of the even family but turns out to be special.

IV. PHASE DIAGRAM OF HALF-FILLED SPIN-3/2 FERMIONS ($N = 2$)

In this section, we give the phase diagram of model (1) when $N = 2$ in the $(U/t, V/t)$ plane, obtained from numerical calculations. Four phases are found and reported in Fig. 8: two phases which break translational invariance, the SP and CDW phases, and two with nondegenerate GS which can only be distinguished through nonlocal string orders, the HI and RS phases. These phases are separated by transition lines determined numerically (solid lines), and compared to weak- and strong-coupling predictions displayed as dashed lines. In addition, three particular lines are plotted where the model has an *exact* enlarged symmetry, which we discussed in Sec. II.

The numerical calculations are performed with DMRG on chains, each site containing the 16 states of the onsite basis (for $N > 2$, since the local Hilbert space is too large, we must use other strategies as discussed below). We fix three quantum numbers: the spin part $S^z = \frac{1}{2}\sum_{\alpha,i}(-1)^{\alpha+1} n_{\alpha,i}$, $T^z = \frac{1}{2}\sum_i (n_{1,i} + n_{2,i} - n_{3,i} - n_{4,i})$, as well as the total number of particles $N_f = 2L$, that is, the total charge. The GS lies in the $S^z = T^z = 0$ sector. The number of kept states is typically $m = 2000$ and OBC are used if not stated otherwise. Denoting by L the length of the chain, the local order parameters are computed numerically by taking their value in the bulk of the chain (we choose to work with an even number of sites):

$$\mathcal{O}_{\mathrm{CDW}}(L) = n_{L/2} - n_{L/2-1}, \tag{72}$$

$$\mathcal{O}_{\mathrm{SP}}(L) = t_{L/2} - t_{L/2-1}, \tag{73}$$

where $n_j = \sum_\alpha n_{\alpha,j}$ is the total onsite density and $t_j = \sum_\alpha c^\dagger_{\alpha,j+1} c_{\alpha,j} + \mathrm{H.c.}$ the local kinetic energy on bond $(j, j+1)$.

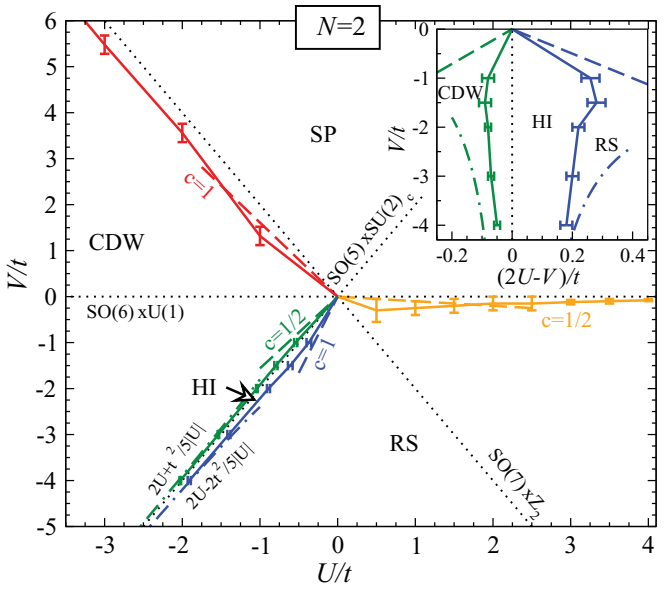

FIG. 8. (Color online) Phase diagram of the $N = 2$ case. Solid lines are DMRG results (see text for discussion) and dashed lines are results from solving numerically the RG flow in the weak-coupling limit. c stands for the expected central charge on the transition line. Lines with higher symmetries are indicated in black dashed lines. Boundaries of the HI phase obtained by the strong-coupling are shown in dotted lines. As a rule of thumb, DMRG results can be trusted if $|U|, |V| \gtrsim t$, while weak-coupling predictions are exact close to the free fermions limit at the origin. (Inset) Zoom on the region of the HI phase where the x axis $(2U - V)/t$ is perpendicular to the $\mathrm{SU}(2)_c \times \mathrm{SO}(5)$ line.

A. The HI phase

We start a more detailed discussion of the phase diagram from the $V = 2U$ line which shows the remarkable $\mathrm{SU}(2)_c$ symmetry, leading to the effective spin-1 Heisenberg model (15) in terms of charge degrees of freedom. We have recently demonstrated[15] that the gapped HI phase is realized for a given value of V/t and that its extension is rather small. We here refine the description of the boundaries of the Haldane phase and discuss the nature of the transition lines to, respectively, the CDW and RS phases. In order to find the transition line from CDW to HI, we use $\mathcal{O}_{\mathrm{CDW}}$ which vanishes in the HI phase and which is straightforward to compute. The transition from HI and RS is more difficult to determine as no local order parameter can discriminate between the two phases. In Ref. 15, we gave several signatures of the transition which can be used to locate it: nonlocal charge string order parameters and the presence of edges states, which are observed here by considering a charge excited state with two additional fermions; for OBC, this state has a vanishing gap to the GS. The simplest way to determine the transition with our numerical scheme is to look at the distribution of the charge in the excited state with $N_f = 2L + 2$: An excess $N_f = 1$ charge will be stuck at each edge in the HI phase (equivalent to the spin-1/2 edge state of the spin-1 Haldane phase), while an $N_f = 2$ excitation lies in the bulk of the RS phase (equivalent to the $S = 1$ magnon of the Heisenberg ladder). We thus use this change in the density profile of the charge excited

state (benchmarked with other signals of the transition for $V = -2t$) to give the estimate of the transition line in Fig. 8.

In the weak-coupling regime, $|U|,|V| \lesssim t$, DMRG calculations become hard due to the relevance of many low-energy onsite states. In the strong-coupling limit (large U,V), onsite energy scales are well-separated so that DMRG efficiently eliminates high-energy irrelevant states. The numerical predictions of the RG flow provides a better prediction for the transition lines in this weak-coupling regime: These estimates are $V \simeq 3.33U$ for RS-HI and $V = 1.56U$ for CDW-HI.

The two transition lines in Fig. 8 are also compared to the strong-coupling predictions of Sec. II B. For large $|U|/t$ and $|V|/t$, the effective Hamiltonian around the SU(2)$_c$ line is a spin-1 model with antiferromagnetic coupling $J = 2t^2/5|U|$ and anisotropy $D = 2U - V$ [see Eqs. (15) and (16)]. The phase diagram of this model has been extensively studied[4,45,79–81] and shows that a Haldane-Néel transition (equivalent to the HI-CDW one) occurs for $D/J \simeq -0.5$ while a Haldane-large-D transition (equivalent to the HI-RS one) is obtained for $D/J \simeq 1$. This gives the two curves, $V_{\text{HI-CDW}} = 2U + t^2/|U|$ and $V_{\text{HI-RS}} = 2U - 2t^2/|U|$, explaining both the shrinking and the asymmetry of the extension of the HI phase in the strong-coupling regime.

Although the Haldane gap decreases in the strong-coupling regime simply because J decreases, the agreement between the fermionic spin-3/2 Hubbard model under study and the spin-1 effective model improves as irrelevant degrees of freedom are pushed to high energies. This can be illustrated numerically by the behavior of the Haldane gap along the SU(2)$_c$ line as a function of U/t. The Haldane gap is computed using OBC from the following gaps:

$$\Delta_{ab} = E_0(2L + 2b) - E_0(2L + 2a), \tag{74}$$

where $E_0(N_f)$ stands for the GS energy with N_f fermions. As evoked previously, the presence of edge states with OBC makes the first excited state collapse onto the GS, so that Δ_{01} vanishes in the thermodynamical limit. Still, both Δ_{02} and Δ_{12} must remain finite and tend to the bulk Haldane gap for sufficiently large sizes. These behaviors, together with finite-size extrapolations of the gaps using the ansatz

$$\Delta_{ab}(L) = \Delta_{ab}(\infty) + \text{const}\, e^{-L/\xi}/L, \tag{75}$$

are clearly shown by the numerical results of Fig. 9(a). Figures 9(b) and 9(c) display the extrapolated gaps as a function of U/t in units of, respectively, t and J. While the weak-coupling opening of the gap cannot be reliably studied here, we observe that the gap passes through a maximum around $U/t \simeq -1$, which is close to value $U/t \simeq -1.5$ for which the width of the HI phase is maximal. In the strong-coupling regime, the gap in units of t decreases as expected [see Fig. 9(b)], while, put in units of J [see Fig. 9(c)], it eventually reaches the value $\Delta_{S=1} \simeq 0.41J$ known[17] for the spin-1 Heisenberg chain: $U \simeq -4t$ is already deep in the strong-coupling regime along this SU(2)$_c$ line.

Last, we investigate the nature of the critical points at the two boundary lines of the HI phase. From the low-energy results of Sec. III B, we expect that the HI-CDW is an Ising transition with a central charge $c = 1/2$, while the HI-RS transition belongs to the BKT type, associated with a central

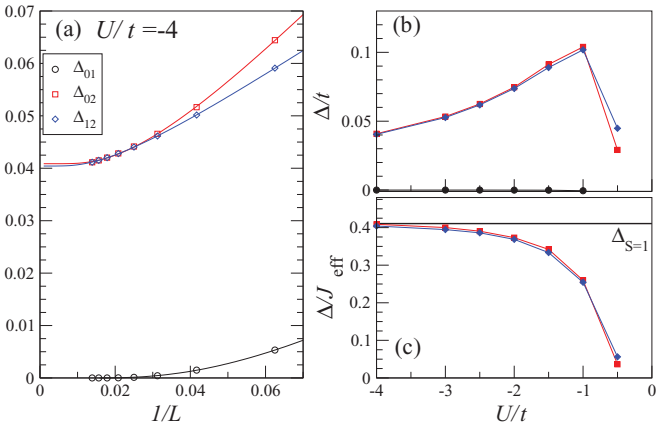

FIG. 9. (Color online) Behavior of the Haldane gap Δ along the SU(2)$_c$ line $V = 2U < 0$ of Fig. 8. (a) Gaps and finite-size scalings (see text for discussion). (b),(c) The Haldane gap as a function of U/t in units of, respectively, t and the effective antiferromagnetic coupling J. The $\Delta_{S=1}$ line indicates the value of the gap known for a Heisenberg spin-one chain.

charge $c = 1$. In the strong-coupling limit, this has been observed numerically for the spin-1 chain with single-ion anisotropy.[80] To check these predictions from the DMRG data, we use the universal scaling of the entanglement entropy (EE) in a critical phase, which gives a direct access to the central charge. We obtained the most convincing results using periodic boundary conditions (PBC) at the price of keeping a much larger number of states and using small system sizes. Similar calculations have been performed in the context of the SU(N) generalization of Haldane's conjecture.[82] The results of the EE on a finite chain of length $L = 48$ along the $V = -2t$ around the HI phase are given in Fig. 10. The central charge is obtained from the data using the universal formula[83]

$$S(x) = \frac{c}{3} \ln d(x|L + 1) + \text{const}, \tag{76}$$

with $d(x|L) = \frac{L}{\pi} \ln(\frac{\pi x}{L})$ the cord function and $S(x)$ the EE of a block of size x with the rest of the chain. The values

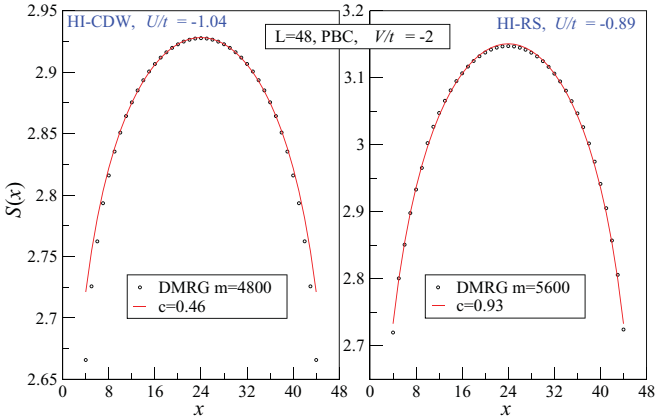

FIG. 10. (Color online) Fitting the entanglement entropy close to the critical lines surrounding the Haldane phase provides central charges c close to the expected values $c = 1/2$ (for HI-CDW) and $c = 1$ (for HI-RS). The best agreement is found using PBC with DMRG and keeping a large number of kept states m.

obtained for c are in good agreement with the expected values considering the large number of local degrees of freedom. There is an uncertainty on the location of the critical points but, on a finite system, as long as $L \ll \xi$, with ξ the correlation length associated to the closing gap, the physics will be effectively that of the critical point.

B. The RS-SP transition

We now turn to the discussion of the RS-SP transition in the right-down quadrant of Fig. 8. The two phases RS and SP can be simply distinguished by the local spin-Peierls order parameter $\mathcal{O}_{\mathrm{SP}}$, which is finite in SP, while it is zero in RS. The vanishing of the order as the system size increases provides a good estimate of the transition line.

We further try to give evidence for the nature of the transition and check whether it lies in the Ising universality class. A possible approach is to use the EE again and look for $c = 1/2$. However, the $\mathcal{O}_{\mathrm{SP}}$ order parameter appears as the leading corrections to the EE with OBC and gives strong oscillations in the signals, particularly in the SP phase and up to the critical point. These oscillations render the fits difficult, and the value of c is not reliably extracted for the accessible system sizes. Using PBC improves a bit the situation, but the oscillating parts of the EE could not be suppressed (as expected for the GS) with DMRG, even by increasing the number of kept states and sweeps.

Consequently, we use another strategy to identify the Ising universality class. We know that the correlation function of the order parameter has a universal exponent $1/4$ at the critical point. Then, Friedel oscillations of the order parameter gives the scaling $\mathcal{O}_{\mathrm{SP}}(L) \propto L^{-1/8}$ on the critical point. In the SP phase, $\mathcal{O}_{\mathrm{SP}}(L)$ reaches a constant in the thermodynamic limit, while it decreases exponentially in the RS phase. Thus, by looking at the scaling of $\mathcal{O}_{\mathrm{SP}}(L)$ for different parameters, we are able to give both a precise estimate of the critical point and to check that the exponent is indeed close to $1/8$. The results along two cuts at $U = 4t$ and $U = t$ are reported in Fig. 11. In the strong-coupling regime $U = 4t$, we do observe a very good agreement with an exponent $1/8$, typical of the Ising universality class. However, in the weak-coupling regime, a much larger exponent of $0.78 \simeq 6/8$ fits well the scaling curves. We understand this discrepancy in the following way: In the weak-coupling regime, the gaps to higher excited states are too small to be thrown away in the low-energy regime of a *finite* system. In other words, the correlation lengths associated with theses gaps become too large and we could not reach sizes sufficiently large to freeze them. A speculative picture can account for the observed number: At weak coupling, the transition line gets very close to the SO(6) line, which has the equivalent of six gapped Ising degrees of freedom, but with an exponentially small gap of the order t/U.[37] In this weak-coupling regime, the numerics cannot resolve these gaps and the Ising degrees of freedom appear critical, each contributing to $1/8$ in the exponent, which then should be close to $6/8$.

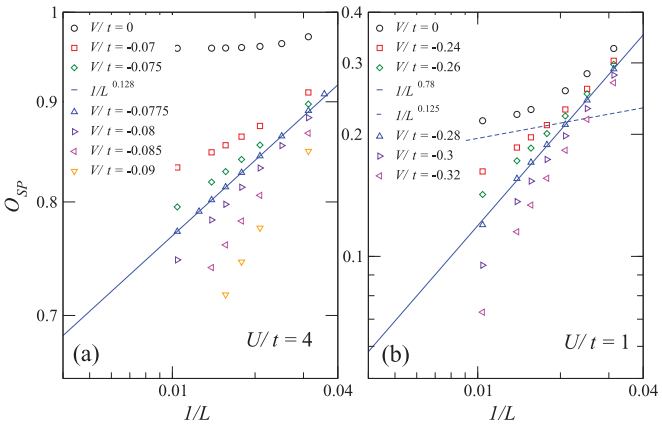

FIG. 11. (Color online) Scaling of the order parameter $\mathcal{O}_{\mathrm{SP}}$ at the RS-SP transition. (a) For $U/t = 4$, the exponent is quite close to $1/8$; (b) for $U/t = 1$, it is closer to 0.8.

This comment brings us to the discussion of effect of the proximity of the SO(6) line (an exact enlarged symmetry) to the RS-SP transition line. The $V = 0$ and $U > 0$ line has been studied analytically and numerically in Ref. 37: The charge and spin gaps open slowly with U/t and are numerically negligible below $U \simeq 2t$. In the weak-coupling regime, the low-energy physics has an emerging enlarged SO(8) symmetry. In the strong coupling regime, the spin gap decreases after passing through a maximum around $U \simeq 6t$. The data shows that the RS-SP transition line has a nonmonotonic behavior, first following the weak-coupling RG predictions and then being attracted by the SO(6) line at large interactions (see Fig. 8). This attraction can be qualitatively understood by the behavior of the spin gap as U increases. Considering V as a perturbation which closes the spin gap Δ_S, the line should typically behave as $V_c(U) \sim -\Delta_S(U)$ which is nonmonotonous and stick to the SO(6) line in the strong-coupling limit. In the weak-coupling limit $U \lesssim t$, the RG prediction $V = -0.10U$ is more reliable than the numerics.

C. The CDW-SP transition

Last, we briefly discuss the CDW-SP transition between these two phases which breaks translational symmetry. Numerically, the precise determination of the transition with $\mathcal{O}_{\mathrm{SP}}$ and $\mathcal{O}_{\mathrm{CDW}}$ using DMRG turns out to be difficult due to formation of domains of each kind of orders close to the transition line. Changing the number of kept states, the number of sweeps and the size, slightly moves the transition point determined by the order parameter at the center of the chain. This leads to error bars in the phase diagram which are relatively small compared to the parameter scales of Fig. 11, but are too large to focus on the critical features of the transition line. We could not check the $c = 1$ expectation of this transition, due to both the difficulty in locating the transition point, and because of strong SP oscillations in the EE. Notice that on the critical line, the correlations of the quartet operator $c^\dagger_{1,i} c^\dagger_{2,i} c^\dagger_{3,i} c^\dagger_{4,i}$ become critical which is qualitatively in agreement with numerical observations.

Here again, we see that the transition line is rather close to a high symmetry line of the phase diagram, namely, the SO(7) line $V = -2U$.[21] In the weak-coupling regime, the numerical solution of the RG Eqs. (30) for $N = 2$ gives $V = -1.61U$ but, for larger $|U|$, DMRG calculations indicate that the transition is attracted to the vicinity of the SO(7) line. An argument similar

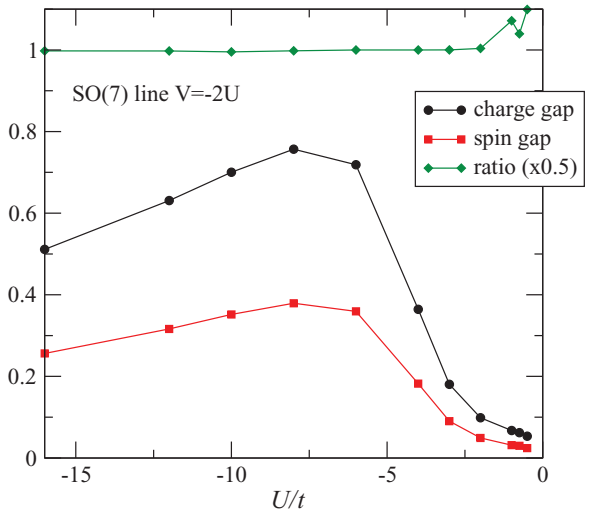

FIG. 12. (Color online) Charge and spin gaps and their ratio along the SO(7) line $V = -2U$ of Fig. 8.

to the one used for the RS-SP transition can be drawn: We see that SO(7) line is in a SP gapped phase. The strong-coupling spin-model along this line is an SO(7) Heisenberg model where the spins belong to the vectorial representation of SO(7)[21] and our analysis predicts a SP bond ordering. Numerically, we compute the spin gap Δ_s and charge gap Δ_c defined as follows:

$$\begin{aligned}\Delta_s &= E_0(N,1) + E_0(N,-1) - 2E_0(N,0),\\ \Delta_c &= E_0(N+2,0) + E_0(N-2,0) - 2E_0(N,0),\end{aligned} \tag{77}$$

where $E_0(N_f, S^z)$ is the GS energy with N_f fermions in the S^z sector with $T^z = 0$ and $N = 2L$ is the reference number of particle at half filling. The results extrapolated in the thermodynamic limit are given in Fig. 12 for a wide range of U/t values. The gaps open slowly in the weak-coupling regime and then reach a maximum around $U \simeq -7t$, before decreasing in the strong-coupling regime. The ratio of the gaps Δ_c/Δ_s is very close to 2, everywhere but in the weak-coupling limit where the numerics are challenging for accurate predictions.

V. PHASE DIAGRAM IN THE $N = 3$ CASE

In this section, we investigate the phase diagram of model (1) when $N = 3$ and in the $(U/t, V/t)$ plane using extensive DMRG simulations. Since the local Hilbert space on each site contains $2^6 = 64$ states and is quite large, we have implemented the following strategy: We use a mapping to a three-leg Hubbard ladder where the chains correspond to fermionic states with S_z equal to $\pm 1/2$, $\pm 3/2$, and $\pm 5/2$, respectively. Then, after some algebra, we can rewrite all hoppings and interaction terms in this language, which introduce, for instance, rung interactions and rung pair-hopping terms. This mapping to a ladder allows us to converge faster to the GS, but we have checked that the symmetry between chains is preserved in the SU(3) case, for instance. Typically, we keep between 1600 and 2000 states in our simulations for measuring local quantities and up to 3000 for correlations, and we use OBC.

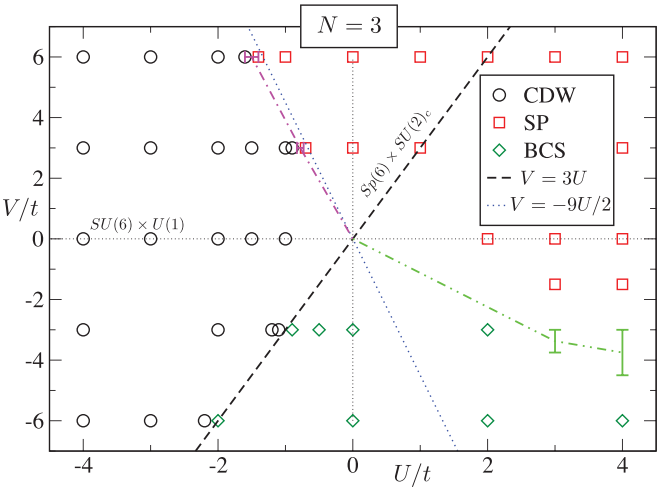

FIG. 13. (Color online) Numerical phase diagram obtained by DMRG in the $N = 3$ case.

Since no topological phase is expected, we can rely on measuring local quantities such as local density and kinetic energy, as well as density and pairing correlations that will characterize the critical phase that has been shown to exist along the $SU(2)_c$ line $V = 3U$ in Ref. 15. The following phase diagram can thus be obtained in Fig. 13 and it contains only three phases: SP, gapless BCS, and CDW.

Data points on this plot correspond to simulations done on system length $L = 72$, while phase boundaries were also obtained from scaling different system sizes (see below).

A. Properties along the $SU(2)_c$ line

We start by considering the $SU(2)_c$ line $V = 3U$. For large enough $|U|/t$, the strong coupling argument of Sec. II B tells us that the chain will behave effectively as an antiferromagnetic Heisenberg spin-3/2 chain, which is known to be critical. In Fig. 14(a), we show how pairing and density correlations behave along this $SU(2)_c$ line. Their long-distance form has

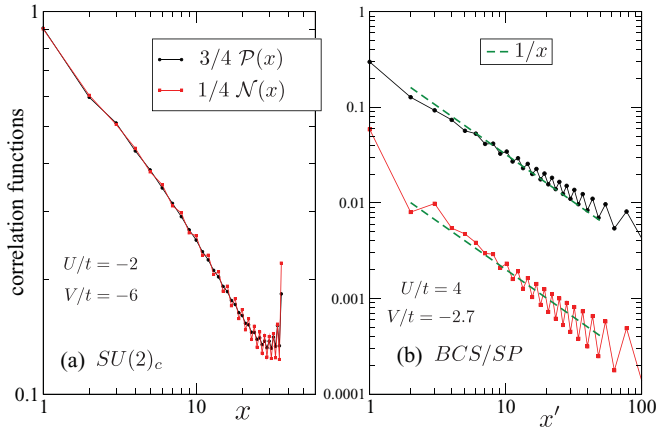

FIG. 14. (Color online) Pairing and density correlations obtained by DMRG in the $N = 3$ case for various interactions corresponding (a) to the exact $SU(2)_c$ symmetry and (b) to the emergent SU(2) symmetry $\widetilde{SU(2)}_c$. Note that correlations are measured starting from the middle of the chain.

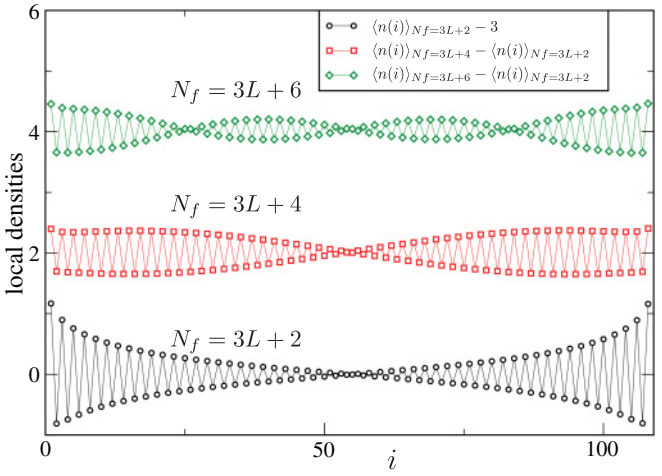

FIG. 15. (Color online) Local densities obtained by DMRG in the $N = 3$ case for $U/t = -2$, $V = 3U$, and $L = 108$. From bottom to top, data correspond to adding two, four, or six particles to the half-filled system. Data for adding four and six particles are shifted by two and four, respectively for clarity, and in these cases $\langle n(i)\rangle_{N_f=3L+2}$ has been substracted in order to get the bulk contribution.

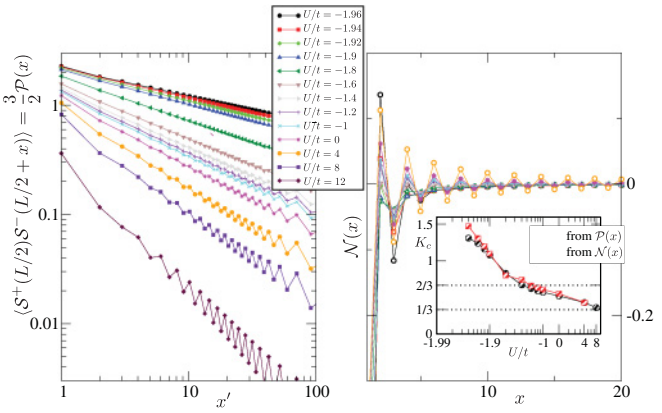

FIG. 16. (Color online) Pair and density correlations in the $N = 3$ case for $V/t = -6$ and $L = 72$ and various U/t. (Inset) Fitting these data gives an estimate of the Luttinger parameter K_c vs U/t (using a log scale starting at $U/t = -2$).

been determined in Eq. (59) and, measured from the middle of the chain, reads

$$\mathcal{P}(x) = \langle P_{00}^{\dagger}(L/2+x)P_{00}(L/2)\rangle \sim \frac{A}{x^{1/(NK_c)}}$$
$$\mathcal{N}(x) = \langle n(L/2+x)n(L/2)\rangle - \langle n(L/2+x)\rangle\langle n(L/2)\rangle$$
$$\sim -\frac{NK_c}{\pi^2 x^2} + \frac{(-1)^x B}{x^{NK_c}}. \quad (78)$$

Using the definition of the pseudospin operator (11), we observe that the two correlations match perfectly, as expected of course for an exact $SU(2)_c$ symmetry. Both correlations are algebraic and expected to decay as $\sqrt{\ln x}/x$,[84] but it is known that checking accurately logarithmic corrections is a challenging numerical problem[85] that we will not further investigate.

Another peculiar property of spin-3/2 chain with OBC was conjectured by Ng[31] and confirmed later numerically:[32] Even though the system is critical, one can observe "edge states" with OBC, in the sense that the magnetization profile will exhibit an excess close to the edges, although there are no finite correlation lengths (i.e., the magnetization profile decays algebraically away from the edges). Here we investigate a similar situation, namely, with a charge $SU(2)_c$ symmetry where it is the local density that plays the role of the magnetization for actual spin-3/2 chain. When adding two, four, or six particles (with respect to half filling), as shown in Fig. 15, we do observe modulations in the local densities reflecting these edge states. Physically, it means that the first excitation (adding two particles) is an edge excitation, but the next ones correspond to making a *bulk* excitation.

B. The transition from critical BCS to SP

As can be seen from the phase diagram shown in Fig. 13, the critical phase that exists along the $SU(2)_c$ line has a rather large extension. As is shown below, this critical phase has dominant BCS pairing correlations; thus its name. For fixed negative V, we observe the transition to the SP phase for large-enough $U > 0$. This is in agreement with the low-energy prediction and the RG phase diagram (see Fig. 6).

In order to characterize the critical phase, we can compute its Luttinger parameter K_c from the behavior of either pairing or density correlations, using Eq. (78). In Fig. 16, we plot both correlations at $V = -6t$ and for various values of U. Let us start with the discussion of $\mathcal{P}(x)$ (which corresponds up to a factor 2/3 to the transverse pseudospin correlation function). In order to be able to fit over the whole range,[86] data are plotted vs $x' = d(x|L+1)/\sqrt{\cos[\pi x/(L+1)]}$, where $d(x|L+1)$ is the cord function, defined in Eq. (76). We observe a very smooth behavior, which makes it possible to extract the behavior of K_c vs U (see inset). Due to the logarithmic corrections which are known to exist along the $SU(2)_c$ line, it is very hard to recover that $K_c \to 1/3$ when $U \to -2t$ as expected from the exact $SU(2)_c$ symmetry. Moving away from the $SU(2)_c$ line, our data indicate that K_c rapidly reaches a maximum, before going down again. The transition to SP corresponds to pairing correlations that become exponential (not shown) and occurs when $K_c = 1/3$ in agreement with the low-energy approach.

Another way to compute K_c consists of using Eq. (78) for density correlations. In principle, one can use either the uniform or the alternating part to extract it. However, in the regime where $K_c < 2/3$, the alternating part is dominant, whereas in the opposite case, the uniform part decays more slowly. Therefore, we have fitted either the uniform part or the staggered part to extract the value of K_c shown in the inset.

Overall, we have an excellent agreement between the estimates of K_c obtained from both correlations, which gives confidence in the validity of the Luttinger liquid description of this critical phase. Moreover, the behavior of K_c vs U is compatible with our expectation (see Sec. III D 3): K_c exceeds 1/3 in the BCS phase (giving rise to dominant BCS correlations) and the transitions to SP and CDW occur when K_c reaches 1/3.

In the critical phase, the von Neumann block entropy gives access to the central charge c, and is consistent with a $c = 1$ Luttinger liquid, as expected (data not shown). In the gapped

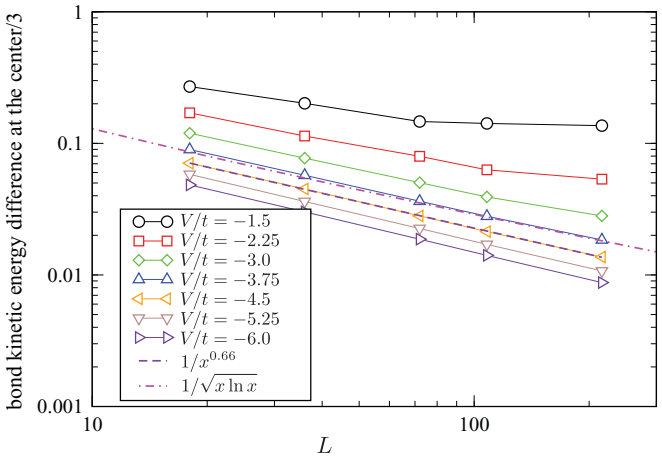

FIG. 17. (Color online) Bond kinetic energy modulation at the center of a chain of length L for various V at fixed $U/t = 3$.

SP phase, the EE scaling is consistent with a saturation for large blocks.

The transition from the critical BCS to the SP phase can be located when $\mathcal{P}(x)$ becomes exponential, or by looking at the bond kinetic modulation scaling. In Fig. 17, we plot the bond kinetic energy difference at the center of the chain as a function of the chain length L. We can clearly see a finite value in the SP phase for $V/t = -1.5$ and $U/t = 3$, for instance, while our data are compatible with an algebraic power-law with exponent 0.66 for larger $|V|$. Locating precisely the transition is difficult since we expect a BKT behavior at the transition, and a weakly opening gap when entering the SP phase; this results in some uncertainty on this transition line in the phase diagram. Using this procedure, we have determined approximately the phase transition line shown in Fig. 13. Although our data are not very accurate, our numerical findings are in agreement with the low-energy approach: The BCS to SP transition occurs for a *finite* negative V for fixed $U > 0$.

Note that the low-energy approach predicts that the transition occurs when K_c reaches $1/3$. According to our fitting procedure (see Fig. 16), this gives a similar estimate for its location. According to this value, the bond kinetic energy modulation should scale as $1/\sqrt{L}$ at the transition, while we have measured a different exponent. In fact, it is known that logarithmic corrections are expected at this transition, and indeed our data can as well be fitted with a $1/\sqrt{L \log L}$ law.

Moreover, along this transition line and from the low-energy approach, we expect an emergent SU(2) symmetry [$\mathrm{SU}(2)_c$] that should be reflected in identical exponents for $\mathcal{P}(x)$ and $\mathcal{N}(x)$. Fig. 14(b) displays our data in this region, and we do confirm a good agreement between the two exponents (compatible with $K_c = 1/3$).

Concerning the transition from the critical BCS to the CDW phase, our data are compatible with a gap opening as soon as $V > NU$, in perfect agreement with the low-energy prediction (see Sec. III D 3). Finally, for the same reasons as in the $N = 2$ case (see Sec. IV C), we could not investigate the nature of the quantum phase transition between SP and CDW phases. We found that this transition is located in the vicinity of the $V = -9U/2$ line (see Fig. 13). Unfortunately, as already stressed in Sec. II, we were not able to determine the symmetry contents of this line.

As a final remark about the BCS phase, while quasiedge states can be observed along the $\mathrm{SU}(2)_c$ line or close to it (see previous section), they no longer exist deep in the BCS phase (for instance $U/t = 0$ and $V/t = -6$, data not shown). This might be understood from the strong-coupling regime using the mapping to a spin-3/2 chain with single-ion anisotropy: For large enough $D > 0$, the relevant low-energy states consist of $S_i^z = \pm 1/2$ on each site, thus leading to an effective spin-1/2 chain in its critical phase. In this region, we do not expect any edge physics as is observed numerically. We have not investigated in details the crossover between both regimes, but it could be easily answered by studying directly a spin-3/2 anisotropic chain.

VI. PHASE DIAGRAM IN THE $N = 4$ CASE

In this section, we investigate the phase diagram of model (1) when $N = 4$ and in the $(U/t, V/t)$ plane.

From a technical point of view, since the local Hilbert space is quite large, we map the 1D model onto a generalized four-leg Hubbard ladder with generalized rung interactions. Thus, we reduce the complexity of the DMRG algorithm, but we have to use a 1D path going along the ladder. We have checked that the symmetry between the chains is always restored during the simulations. Typically, we keep 2000 states in our simulations and use OBC.

Figure 18 shows the phase diagram for $N = 4$, obtained on a $L = 30$ chain. As expected, five phases are present: On the $\mathrm{SU}(2)_c$ line in the attractive part of the phase diagram, there is the HI phase and, close to it, the critical BCS one arises. As expected from the strong-coupling argument [see Eq. (15)], it is followed by the RS phase and, on the other side of the HI phase, a CDW phase is stabilized. On the repulsive side, we detect a SP phase that was predicted in Sec. III C. We observe a good agreement with the low-energy prediction (see Fig. 7).

A. Properties along the $\mathrm{SU}(2)_c$ line

We start by looking at the $\mathrm{SU}(2)_c$ line $V = 4U$ on the attractive side. As expected from the strong-coupling argument and from the low-energy analysis, the model should behave as

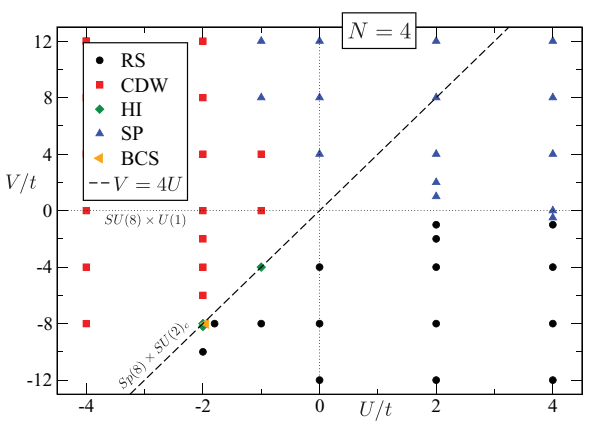

FIG. 18. (Color online) Numerical phase diagram obtained by DMRG in the $N = 4$ case with $L = 30$.

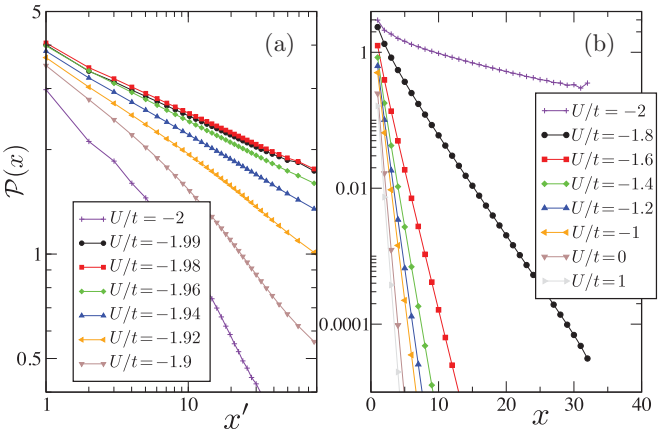

FIG. 19. (Color online) Pairing correlations for $N = 4$ at fixed $V/t = -8$ and $L = 64$. (a) Critical correlations are observed close to the HI phase represented by $U/t = -2$ on the SU(2)$_c$ line. (b) Both in HI and in RS phase, the pairing correlations are short ranged.

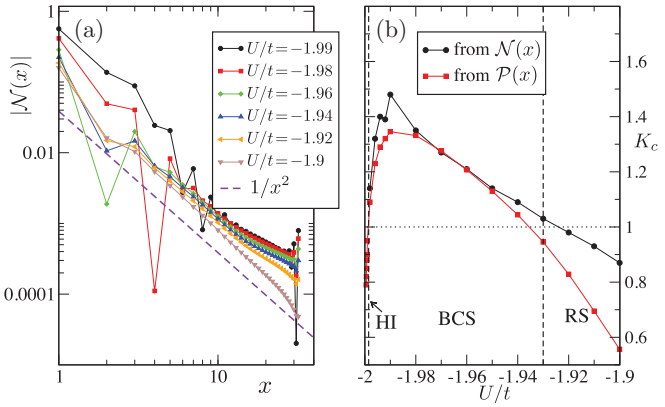

FIG. 20. (Color online) (a) Density correlations for $N = 4$ at fixed $V/t = -8$ and $L = 64$ in the BCS phase. (b) Luttinger liquid parameter K_c vs U for fixed $V/t = -8$. BCS phase is delimited by $K_c \geqslant 1$.

an effective antiferromagnetic spin-2 Heisenberg chain, that is, be in a Haldane phase.

We have some evidence for such a HI phase thanks to the presence of (charge) edge states when OBC are used. Concerning the charge gap, in order to get the bulk result (and avoid edge states effect), one needs to compute $E_0(N_f = 4L + 6) - E_0(N_f = 4L + 4)$. Extrapolating our data on $L = 16$ and $L = 32$ chains for $U = -2t$ and $V = -8t$, we obtain an estimate of $0.0038t$, which is extremely small. Nevertheless, using the strong-coupling expression of the effective exchange $J_{\text{eff}} = 1/18t$ and the known Haldane gap[87] $\Delta \simeq 0.089 J_{\text{eff}} \simeq 0.0049t$, we get a finite gap of the same magnitude.

Moreover, the pairing correlations (which correspond to the transverse spin correlations in the spin language) shown in Fig. 19 exhibit a short-range behavior compatible with a finite correlation length and a finite gap.

However, since the correlation length of the spin-2 chain is known to be very large[87] ($\xi \sim 50$), we will not try to characterize further this HI phase (by measuring its string order, for instance), but the strong-coupling argument ensures that HI phase exists in some finite region of the phase diagram around the SU(2)$_c$ line.

B. Critical BCS phase

In Sec. II B, we have argued why, for fixed V/t, increasing U/t gives an effective single-ion anisotropy denoted D. For the spin-2 chain, it is known[68] that such a D term leads to an *extended* critical XY phase with central charge $c = 1$ for $0.04 < D/J_{\text{eff}} < 2.4$. Using our strong-coupling estimate and assuming a fixed effective J_{eff}, this would predict an extended XY phase for $-1.996 < U/t < -1.82$ for fixed $V/t = -8$.

Figure 19 shows numerical data for the pairing correlations obtained for a chain with $L = 64$. Indeed, algebraic behavior is observed close to the Haldane phase, in a region corresponding to $-1.99 \lessapprox U/t \lessapprox -1.9$ for $V = -8t$, in agreement with our strong-coupling estimate.

In order to be more quantitative about this Luttinger liquid phase, and make a connection with the low-energy analysis, we use the asymptotics from Eq. (70),

$$\begin{aligned}\mathcal{P}(x) &= \langle P_{00}^{\dagger}(L/2+x) P_{00}(L/2)\rangle \sim x^{-1/NK_c} \\ \mathcal{N}(x) &= \langle n(L/2+x) n(L/2)\rangle - \langle n(L/2+x)\rangle\langle n(L/2)\rangle \\ &\sim -\frac{NK_c}{\pi^2 x^2} + (-1)^x A \exp(-x/\xi), \end{aligned} \tag{79}$$

and use it to extract the behavior of K_c in the $c = 1$ gapless phase. Note that we have measured the correlations from the center of the chain in order to minimize size effects due to OBC, and in the critical phase, we plot our data vs $x' = d(x|L+1)/\sqrt{\cos[\pi x/(L+1)]}$ in order to be able to fit over the whole range.[86]

Density correlations are shown in Fig. 20(a) in the critical phase, and they exhibit an algebraic decay. The anomalies are due to the subleading short-range staggered contributions since we plot the absolute values of $\mathcal{N}(x)$, so that density correlations become difficult to fit close to the HI phase. We have fitted both correlations using the expressions above in Eqs. (79) and the resulting Luttinger parameter K_c is plotted in Fig. 20(b). We have an overall good agreement between the two *independent* fits, and we confirm the expected behavior that, starting from the HI phase, K_c first increases rapidly, and then diminishes when U/t increases. The gapless phase is characterized by $K_c \geqslant 1$, which corresponds for $V/t = -8$ to $-1.999 \leqslant U/t \leqslant -1.93$. Thus, we conclude, from Eqs. (79), that the leading instability is the BCS singlet-pairing. The extended gapless phase is thus a BCS phase which differs from the one in the $N = 3$ case by the fact that the staggered part of the density is short-ranged.

For the choice of $V/t = -8$, we see that both pairing and density correlations become short-range when $U/t \gtrapprox -1.9$, where a RS (large-D) phase starts. As can be seen from the behavior of K_c, this corresponds to $K_c = 1 = 4/N$, which is the criterion for the opening of the gap in the bosonization analysis done in Sec. III D 4.

C. Quantum phase transitions

Once we have determined the five phases in the phase diagram, we would like to clarify the nature of the quantum phase transitions.

Starting from the $SU(2)_c$ line with $V < 0$ and decreasing U leads to a CDW phase. According to the low-energy approach, and as confirmed numerically for $N = 2$, we expect a $c = 1/2$ second-order Ising phase transition. However, due to the large correlation length in the HI phase, we cannot get reliable results. It would be much easier to check this criticality, as well as locate the critical D/J, by studying directly the spin-2 chain with single-ion anisotropy.

On the other side of the HI phase, that is, increasing U, the phase transition to BCS critical phase was predicted to be in the BKT universality class with $c = 1$. Scaling of EE for $L = 64$ with $V/t = -4.0$ and $U/t = -0.9$ leads to $c = 0.93$ (when keeping $m = 4000$ states in the DMRG simulation). From the BCS phase and increasing U/t at fixed $V/t < 0$, our correlation functions in Figs. 19 and 20 are compatible with a transition to a fully gapped RS phase when K_c becomes smaller than 1, as expected.

The transition from RS to SP is difficult to characterize due to finite-size oscillations in the quantities (including EE), but we have determined that it is located at a *finite* negative V for fixed $U > 0$ as found in the low-energy section (see Fig. 7). A similar conclusion can be made for the transition from SP to CDW, which is located in the opposite quadrant, as expected.

VII. CONCLUSION

We have established the zero temperature phase diagram of multicomponent ($2N$-component) fermionic cold atoms, loaded in a 1D optical lattice, at half filling. This entire work was done under the hypothesis that only contact interactions matter and that the interactions channels can be reduced to two: one singlet channel and one nonzero spin channel. The former hypothesis is very reasonable in the context of optical lattices and could be relaxed without affecting our main conclusions. The latter hypothesis requires $N - 2$ independent fine-tunings, and is therefore quite restrictive for large N. However, it requires no fine tuning for $N \leqslant 2$, and should not be out of reach for moderate $N \leqslant 4$.

As soon as $N > 1$, we found that the phase diagram has a rich structure due to the degeneracy of the atomic states and the absence of spin-charge separation at half filling. Several nonequivalent Mott-insulating phases emerge. Two phases are present irrespective of the value of $N > 1$: the SP and CDW phases, which both break translational invariance and are twofold degenerate. We exhibited a hidden pseudospin SU(2) structure, involving spin-singlet, charged degrees of freedom, that generalizes a structure noticed long ago for the $N = 1$ case in the context of the Hubbard model.[28] When specialized to one space dimension, this structure yields a Haldane conjecture for attractive interactions: We show that such a system realizes a Heisenberg antiferromagnet of magnitude $S = N/2$, and, as a consequence, displays an alternating gapped (insulating)/critical (BCS superfluid) behavior according to the even/odd parity of N. We have found that this parity effect has an influence on large portions of the phase diagram, and that ultracold fermions with N even can disclose two more insulating states: the HI and RS phases which are nondegenerate and display nonlocal string orderings. The $N = 1,2$ cases turn out not to be the generic cases of the odd/even families. Precisely, whereas for $N = 2$, only a critical quantum phase transition occurs between the two nondegenerate insulating phases, for even $N > 2$, an intermediate gapless BCS phase arises between them.

On top of the even-odd scenario, and within the low-energy approach, we found a subtle effect depending on the parity of $N/2$. When $N/2$ is odd, the HI and RS phases correspond to different phases and can be distinguished by string-order parameters. In particular, the HI phase with odd $N/2$, that is, odd spin, is an exemple of a topological ordered phase with $N/4$ edge states. In contrast, when $N/2$ is even, the HI and RS phases are related at low-energy by a duality symmetry and share the same GS properties. In this respect, the HI phase with $N/2$ even, that is, for even spin, is not topologically protected by its edge-state structure but is equivalent to a topological trivial insulating phase, that is, the RS phase. Thus, within the low-energy approach presented in this paper, our findings confirm the recent conjecture of Ref. 33.

In the light of the recent experimental achievements where cold fermionic gases with several components could be stabilized as highly symmetry systems,[88] we hope that it will be possible in the future to unveil part of the richness that we highlighted in this work. In particular, the disclosure of the HI phase would be extremely important, as it displays exotic characteristics that have attracted a lot of attention in the past years and still does nowadays.

ACKNOWLEDGMENTS

The authors would like to thank T. Jolicoeur, K. Totsuka, and P. Azaria for insightful discussions. Numerical simulations were performed using HPC resources from GENCI-IDRIS (Grant No. 2009-100225) and CALMIP.

[1] X. G. Wen, *Quantum Field Theory of Many-Body Systems* (Oxford University Press, London, 2004).
[2] P. W. Anderson, *Basic Notions of Condensed Matter Physics* (Addison-Wesley, Reading, MA, 1984).
[3] F. D. M. Haldane, Phys. Lett. A **93**, 464 (1983); Phys. Rev. Lett. **50**, 1153 (1983).
[4] M. P. M. den Nijs and K. Rommelse, Phys. Rev. B **40**, 4709 (1989).
[5] T. Kennedy and H. Tasaki, Phys. Rev. B **45**, 304 (1992).
[6] M. Hagiwara, K. Katsumata, I. Affleck, B. I. Halperin, and J. P. Renard, Phys. Rev. Lett. **65**, 3181 (1990).
[7] P. Lecheminant, in *Frustrated Spin Systems*, edited by H. T. Diep (World Scientific, Singapore, 2004).
[8] H.-J. Mikeska and A. K. Kolezhuk, Lect. Notes Phys. **645**, 1 (2004).
[9] E. Altman and A. Auerbach, Phys. Rev. Lett. **81**, 4484 (1998).

[10]J. J. Garcia-Ripoll, M. A. Martin-Delgado, and J. I. Cirac, Phys. Rev. Lett. **93**, 250405 (2004).
[11]E. G. Dalla Torre, E. Berg, and E. Altman, Phys. Rev. Lett. **97**, 260401 (2006); E. Berg, E. G. Dalla Torre, T. Giamarchi, and E. Altman, Phys. Rev. B **77**, 245119 (2008).
[12]Y. W. Lee, Y. L. Lee, and M.-F. Yang, Phys. Rev. B **76**, 075117 (2007); Y. W. Lee, *ibid.* **77**, 064514 (2008).
[13]L. Amico, G. Mazzarella, S. Pasini, and F. S. Cataliotti, New J. Phys. **12**, 013002 (2010).
[14]M. Dalmonte, M. Di Dio, L. Barbiero, and F. Ortolani, Phys. Rev. B **83**, 155110 (2011).
[15]H. Nonne, P. Lecheminant, S. Capponi, G. Roux, and E. Boulat, Phys. Rev. B **81**, 020408(R) (2010).
[16]P. Di Francesco, P. Mathieu, and D. Sénéchal, *Conformal Field Theory* (Springer, Berlin, 1997).
[17]S. R. White, Phys. Rev. Lett. **69**, 2863 (1992); Phys. Rev. B **48**, 10345 (1993); U. Schollwöck, Rev. Mod. Phys. **77**, 259 (2005).
[18]T. L. Ho and S. Yip, Phys. Rev. Lett. **82**, 247 (1999).
[19]S. Sachdev and Z. Wang, Phys. Rev. B **43**, 10229 (1991).
[20]C. J. Wu and S. C. Zhang, Phys. Rev. B **71**, 155115 (2005).
[21]C. J. Wu, J. P. Hu, and S. C. Zhang, Phys. Rev. Lett. **91**, 186402 (2003); C. J. Wu, Mod. Phys. Lett. B **20**, 1707 (2006).
[22]P. Lecheminant, E. Boulat, and P. Azaria, Phys. Rev. Lett. **95**, 240402 (2005).
[23]P. Lecheminant, P. Azaria, and E. Boulat, Nucl. Phys. B **798**, 443 (2008).
[24]C. J. Wu, Phys. Rev. Lett. **95**, 266404 (2005).
[25]S. Capponi, G. Roux, P. Azaria, E. Boulat, and P. Lecheminant, Phys. Rev. B **75**, 100503(R) (2007); S. Capponi, G. Roux, P. Lecheminant, P. Azaria, E. Boulat, and S. R. White, Phys. Rev. A **77**, 013624 (2008); G. Roux, S. Capponi, P. Lecheminant, and P. Azaria, Eur. Phys. J. B **68**, 293 (2009).
[26]H.-H. Hung, Y. Wang, and C. Wu, Phys. Rev. B **84**, 054406 (2011).
[27]C. N. Yang, Phys. Rev. Lett. **63**, 2144 (1989).
[28]C. N. Yang and S. C. Zhang, Mod. Phys. Lett. B **4**, 759 (1990); S. C. Zhang, Int. J. Mod. Phys. B **5**, 153 (1991).
[29]A. O. Gogolin, A. A. Nersesyan, and A. M. Tsvelik, *Bosonization and Strongly Correlated Systems* (Cambridge University Press, Cambridge, 1998).
[30]T. Giamarchi, *Quantum Physics in One Dimension* (Clarendon Press, Oxford, 2004).
[31]T. K. Ng, Phys. Rev. B **50**, 555 (1994).
[32]S. Qin, T. K. Ng, and Z. B. Su, Phys. Rev. B **52**, 12844 (1995); J. Lou, S. Qin, T. K. Ng, and Z. Su, *ibid.* **65**, 104401 (2002); J. Lou, S. Qin, and C. Chen, Phys. Rev. Lett. **91**, 087204 (2003).
[33]F. Pollmann, E. Berg, A. M. Turner, and M. Oshikawa, e-print arXiv:0909.4059 (to be published).
[34]T. Tonegawa, K. Okamoto, H. Nakano, T. Sakai, K. Nomura, and M. Kaburagi, J. Phys. Soc. Jpn. **80**, 043001 (2011).
[35]I. Affleck, D. Arovas, J. B. Marston, and D. Rabson, Nucl. Phys. B **366**, 467 (1991).
[36]A. Paramekanti and J. B. Marston, J. Phys. Condens. Matter **19**, 125215 (2007).
[37]R. Assaraf, P. Azaria, E. Boulat, M. Caffarel, and P. Lecheminant, Phys. Rev. Lett. **93**, 016407 (2004).
[38]A. V. Onufriev and J. B. Marston, Phys. Rev. B **59**, 12573 (1999).
[39]K. Buchta, Ö. Legeza, E. Szirmai, and J. Sólyom, Phys. Rev. B **75**, 155108 (2007).
[40]H. Nonne, E. Boulat, S. Capponi, and P. Lecheminant, Phys. Rev. B **82**, 155134 (2010).
[41]J. Zhao, K. Ueda, and X. Wang, Phys. Rev. B **74**, 233102 (2006); J. Phys. Soc. Jpn. **76**, 114711 (2007).
[42]P. W. Anderson, Phys. Rev. **112**, 1900 (1958).
[43]S. Capponi, C. J. Wu, and S. C. Zhang, Phys. Rev. B **70**, 220505 (2004).
[44]A. Auerbach, *Interacting Electrons and Quantum Magnetism* (Springer-Verlag, New York, 1994).
[45]H. J. Schulz, Phys. Rev. B **34**, 6372 (1986).
[46]F. Bais and P. Bouwknegt, Nucl. Phys. B **279**, 561 (1987); A. N. Schellekens and N. P. Warner, Phys. Rev. D **34**, 3092 (1986).
[47]D. Altschuler, Nucl. Phys. B **313**, 293 (1989).
[48]V. G. Knizhnik and A. B. Zamolodchikov, Nucl. Phys. B **247**, 83 (1984).
[49]E. Boulat, P. Azaria, and P. Lecheminant, Nucl. Phys. B **822**, 367 (2009).
[50]D. J. Gross and A. Neveu, Phys. Rev. D **10**, 3235 (1974).
[51]H.-H. Lin, L. Balents, and M. P. A. Fisher, Phys. Rev. B **58**, 1794 (1998).
[52]R. M. Konik, H. Saleur, and A. W. W. Ludwig, Phys. Rev. B **66**, 075105 (2002).
[53]A. B. Zamolodchikov and Al. B. Zamolodchikov, Ann. Phys. (NY) **120**, 253 (1979).
[54]M. Karowski and H. J. Thun, Nucl. Phys. B **190**, 61 (1981).
[55]R. Konik and A. W. W. Ludwig, Phys. Rev. B **64**, 155112 (2001).
[56]C. Ahn, D. Bernard, and A. LeClair, Nucl. Phys. B **346**, 409 (1990).
[57]A. Babichenko, Nucl. Phys. B **697**, 481 (2004).
[58]A. B. Zamolodchikov and V. A. Fateev, Sov. Phys. JETP **62**, 215 (1985).
[59]D. Gepner and Z. Qiu, Nucl. Phys. B **285**, 423 (1987).
[60]I. Affleck and F. D. M. Haldane, Phys. Rev. B **36**, 5291 (1987).
[61]D. C. Cabra, P. Pujol, and C. von Reichenbach, Phys. Rev. B **58**, 65 (1998).
[62]V. A. Fateev, Int. J. Mod. Phys. A **6**, 2109 (1991).
[63]I. Affleck, Nucl. Phys. B **265**, 448 (1986).
[64]P. Lecheminant and E. Orignac, Phys. Rev. B **65**, 174406 (2002).
[65]M. Oshikawa, J. Phys. Condens. Matter **4**, 7469 (1992).
[66]K. Totsuka and M. Suzuki, J. Phys. Condens. Matter **7**, 1639 (1995).
[67]Y. Hatsugai, J. Phys. Soc. Jpn. **61**, 3856 (1992).
[68]U. Schollwöck and Th. Jolicoeur, Europhys. Lett. **30**, 493 (1995); U. Schollwöck, O. Golinelli, and Th. Jolicoeur, Phys. Rev. B **54**, 4038 (1996).
[69]Y. Nishiyama, K. Totsuka, N. Hatano, and M. Suzuki, J. Phys. Soc. Jpn. **64**, 414 (1995).
[70]H. Aschauer and U. Schollwöck, Phys. Rev. B **58**, 359 (1998).
[71]S. Qin, J. Lou, L. Sun, and C. Chen, Phys. Rev. Lett. **90**, 067202 (2003).
[72]I. Affleck, T. Kennedy, E. H. Lieb, and H. Tasaki, Phys. Rev. Lett. **59**, 799 (1987).
[73]K. Totsuka (private communications).
[74]S. K. Yang, Nucl. Phys. B **285**, 183639 (1987).
[75]P. Lecheminant, A. O. Gogolin, and A. A. Nersesyan, Nucl. Phys. B **639**, 502 (2002).
[76]M. Fabrizio, A. O. Gogolin, and A. A. Nersesyan, Phys. Rev. Lett. **83**, 2014 (1999); Nucl. Phys. B **580**, 647 (2000).
[77]G. Delfino and G. Mussardo, Nucl. Phys. B **516**, 675 (1998).
[78]Z. Bajnok, L. Palla, G. Takacs, and F. Wagner, Nucl. Phys. B **601**, 503 (2001).

[79]R. Botet, R. Jullien, and M. Kolb, Phys. Rev. B **28**, 3914 (1983); W. Chen, K. Hida, and B. C. Sanctuary, *ibid*. **67**, 104401 (2003).
[80]C. Degli Esposti Boschi, E. Ercolessi, F. Ortolani, and M. Roncaglia, Eur. Phys. J. B **35**, 463 (2003).
[81]A. F. Albuquerque, C. J. Hamer, and J. Oitmaa, Phys. Rev. B **79**, 054412 (2009).
[82]S. Rachel, R. Thomale, M. Fuhringer, P. Schmitteckert, and M. Greiter, Phys. Rev. B **80**, 180420(R) (2009).
[83]P. Calabrese and J. Cardy, J. Stat. Mech. (2004) P06002; J. Phys. A **42**, 504005 (2009).
[84]I. Affleck, D. Gepner, H. J. Schulz, and T. Ziman, J. Phys. A: Math. Gen. **22**, 511 (1989); R. R. P. Singh, M. E. Fisher, and R. Shankar, Phys. Rev. B **39**, 2562 (1989).
[85]K. Hallberg, X. Q. G. Wang, P. Horsch, and A. Moreo, Phys. Rev. Lett. **76**, 4955 (1996).
[86]M. A. Cazalilla, J. Phys. B **37**, S1 (2004).
[87]S. Todo and K. Kato, Phys. Rev. Lett. **87**, 047203 (2001).
[88]S. Taie, Y. Takasu, S. Sugawa, R. Yamazaki, T. Tsujimoto, R. Murakami, and Y. Takahashi, Phys. Rev. Lett. **105**, 190401 (2010).